C. R. Mecanique 345 (2017) 399–416

Contents lists available at ScienceDirect

Comptes Rendus Mecanique

www.sciencedirect.com

Stochastic modeling and generation of random fields of elasticity tensors: A unified information-theoretic approach

Brian Staber, Johann Guilleminot *

Université Paris-Est, Laboratoire "Modélisation et simulation multi-échelle", MSME UMR 8208 CNRS, 5, bd Descartes, 77454 Marne-la-Vallée, France

ARTICLE INFO

Article history:
Received 26 January 2017
Accepted 5 May 2017
Available online 29 May 2017

Keywords:
Information theory
Maximum entropy principle
Random fields
Elasticity
Stochastic differential equation
Symmetry classes

ABSTRACT

In this Note, we present a unified approach to the information-theoretic modeling and simulation of a class of elasticity random fields, for all physical symmetry classes. The new stochastic representation builds upon a Walpole tensor decomposition, which allows the maximum entropy constraints to be decoupled in accordance with the tensor (sub)algebras associated with the class under consideration. In contrast to previous works where the construction was carried out on the scalar-valued Walpole coordinates, the proposed strategy involves both matrix-valued and scalar-valued random fields. This enables, in particular, the construction of a generation algorithm based on a memoryless transformation, hence improving the computational efficiency of the framework. Two applications involving weak symmetries and sampling over spherical and cylindrical geometries are subsequently provided. These numerical experiments are relevant to the modeling of elastic interphases in nanocomposites, as well as to the simulation of spatially dependent wood properties for instance.

1. Preliminaries

1.1. Introduction

The representation of spatially dependent uncertainties is a cornerstone of predictive simulations. Over the past three decades, this has been mostly achieved, in linear elasticity, by resorting to polynomial chaos expansions (see [1] and the references therein for a recent survey) and algebraic decompositions of random fields. The latter type of approaches includes the selection or construction of models in the class of all admissible second-order stochastic representations, where admissibility typically refers to the fulfillment (with probability one) of all the basic properties raised by the mathematical analysis of the stochastic boundary value problem [2,3]. In three-dimensional linear elasticity, such properties include, for instance, the positive-definiteness of the tensor-valued elasticity coefficient [4]. A contribution involving *a priori* model selection can be found, for instance, in [5] for isotropic materials, while construction methodologies building upon information theory [6,7] and the maximization of Shannon's entropy were proposed in [2,8–11], to list a few. Such models will be referred to as information-theoretic ones below, and define admissible subsets – with a minimal modeling bias – of the set of all second-order elasticity random fields. They enable, in particular, fast numerical simulations for physics-based uncertainty propagation and involve low-dimensional hyperparameters, which allows for an identification solving (underdetermined)

* Corresponding author.
E-mail address: johann.guilleminot@duke.edu (J. Guilleminot).

http://dx.doi.org/10.1016/j.crme.2017.05.001

statistical inverse problems. It should be noticed that a recent theoretical work addressing the modeling (through spectral expansions) of the complete set of elasticity tensors for all symmetry classes can be found in [12].

From a modeling standpoint, a key issue is the representation of anisotropy and the evolution of the latter as the elasticity tensor becomes random. Depending on the retained framework, the sought quantity of interest and computational resources, one may consider random fields of elasticity tensors with fluctuations in a given symmetry class (which may be inferred from microstructural information) or in the triclinic class (see [13] for a micromechanics-based discussion). The latter (triclinic) case was first addressed in [2], making use of earlier derivations proposed in [14] for structural dynamics. The model relies on a random matrix formulation that induces triclinic fluctuations and does not allow other symmetry classes to be considered, due the eigenvalue repulsion phenomenon [15]. Similar ideas were then pursued in [9,10], in which a decomposition onto an *ad hoc* tensor basis was used to circumvent this limitation. This approach involves an exponential map that allows one to relax the algebraic constraints generated by the positive-definiteness and symmetry properties of the tensor (in practice, these constraints can raise critical sampling issues for weak symmetries). Additionally, this construction enables efficient random field sampling through the integration of a family of stochastic differential equations.

In this Note, we show that these two constructions (namely, the one based on the random matrix approach and the one involving the tensorial decomposition) can indeed be unified in a rather simple form. This offers two benefits. First of all, the new random field model exhibits closed-form expressions (for some statistical properties) that are inherited from each stochastic representation and facilitate the calibration of the model hyperparameters. Secondly, the sampling algorithm turns out to be very robust and easy to implement. The model and generator are readily applicable, for instance, to the modeling of composite laminates and wood species (these materials being typically considered as orthotropic in an appropriate local or global coordinate system), and to the representation of bone properties (which may be modeled as a transversely isotropic material) in computational biomechanics.

This Note is organized as follows. The section 2 is concerned with the construction of the stochastic representation. The methodology is first outlined in Sec. 2.1. The definition of the probabilistic model is then addressed in the most general setting in Sec. 2.2. Numerical examples are finally provided in Sec. 3.

1.2. Notation

In this paper, deterministic scalars, vectors, second-order and fourth-order tensors are denoted by d, $\boldsymbol{d}$, $[D]$ and $[\![D]\!]$. Let $\langle\cdot,\cdot\rangle$ denote the Euclidean inner product in $\mathbb{R}^3$, with $\langle \boldsymbol{x}, \boldsymbol{y}\rangle := \sum_{i=1}^3 x_i y_i$ for $(\boldsymbol{x}, \boldsymbol{y}) \in \mathbb{R}^3 \times \mathbb{R}^3$. Let $\mathbb{M}_6^{\mathrm{S}}(\mathbb{R})$ be the set of symmetric real-valued (6×6) matrices. The inner product in $\mathbb{M}_6^{\mathrm{S}}(\mathbb{R})$ is defined as $\ll [U], [V] \gg := \mathrm{Tr}([U][V])$ for any $[U]$ and $[V]$ in $\mathbb{M}_6^{\mathrm{S}}(\mathbb{R})$, and the induced (Frobenius) norm reads as $\|[U]\|_F = \ll [U], [U] \gg^{1/2}$. In addition, let $\mathbb{M}_6^{+}(\mathbb{R}) \subset \mathbb{M}_6^{\mathrm{S}}(\mathbb{R})$ be the set of symmetric positive-definite real-valued (6×6) matrices. The standard tensor product is denoted by $\otimes$, while the symmetric tensor product between second-order tensors is defined component-wise as: $([U] \boxtimes [V])_{ijkl} := (u_{ik}v_{jl} + u_{il}v_{jk})/2$. Let $[I_s]$ be the identity matrix of size s.

Stochastic scalars, vectors and second-order tensors are denoted by D, $\boldsymbol{D}$ and $[\boldsymbol{D}]$ respectively. The mathematical expectations $\mathbb{E}\{D\}$, $\mathbb{E}\{\boldsymbol{D}\}$ and $\mathbb{E}\{[\boldsymbol{D}]\}$ of random variables D, $\boldsymbol{D}$ and $[\boldsymbol{D}]$ are denoted by $\underline{d}$, $\underline{\boldsymbol{d}}$ and $[\underline{D}]$, respectively. The level of statistical fluctuations exhibited by a random matrix $[\boldsymbol{D}]$ is characterized by the parameter $\delta_{[\boldsymbol{D}]}$ defined as

$$\delta_{[\boldsymbol{D}]} := \left\{ \frac{\mathbb{E}\{\|[\boldsymbol{D}] - [\underline{D}]\|_F^2\}}{\|[\underline{D}]\|_F^2} \right\}^{1/2} \tag{1}$$

Note that when applied to a scalar random variable, the above equation coincides with the standard definition of the coefficient of variation. Finally, c_0 denotes the normalization constant involved in probability density functions. The value of c_0 may therefore change from line to line with no specific statement.

2. Construction of the random field model

2.1. Overview of the methodology

Let $\{[\boldsymbol{C}(\boldsymbol{x})], \boldsymbol{x} \in \Omega\}$ be the $\mathbb{M}$-valued random field of elasticity tensor, with $\mathbb{M} \subseteq \mathbb{M}_6^{+}(\mathbb{R})$ and $\Omega \subset \mathbb{R}^3$. The modified Voigt representation of fourth-order tensors is considered (see *e.g.*, [16]), and the elasticity field is expressed in a given Cartesian global coordinate system $\mathfrak{R}_g := (O, \boldsymbol{e}_1, \boldsymbol{e}_2, \boldsymbol{e}_3)$ (with generic variables $\boldsymbol{x}$ and $\boldsymbol{y}$). Regarding the material symmetry exhibited by the material, two practical situations can be envisioned as follows:

- When the symmetry class under consideration is defined by crystallographic orientations that are independent of $\boldsymbol{x}$ in $\mathfrak{R}_g$ (in which case the symmetry properties hold in the global coordinate system), the state space $\mathbb{M}$ is equal to $\mathbb{M}_6^{\mathrm{sym}}(\mathbb{R})$, where $\mathbb{M}_6^{\mathrm{sym}}(\mathbb{R}) \subset \mathbb{M}_6^{+}(\mathbb{R})$ is the set of elasticity matrices belonging to the symmetry class parametrized by the aforementioned preferred directions (note that the dependence of $\mathbb{M}_6^{\mathrm{sym}}(\mathbb{R})$ on these directions is not made explicit in order to simplify notations).

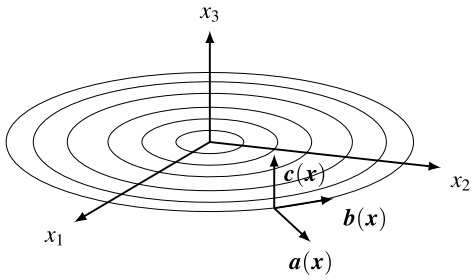

Fig. 1. Illustration of local orthotropy (with crystallographic orientations defined by $\boldsymbol{a}$, $\boldsymbol{b}$ and $\boldsymbol{c}$) for wood materials (here, the ellipses schematically represent the wood rings).

- When the material involves crystallographic orientations that are spatially dependent in $\mathfrak{R}_g$, meaning that the symmetry is indeed exhibited in a local coordinate system (which is denoted by $\mathfrak{R}_\ell$ hereinafter), the state space (with the field expressed in $\mathfrak{R}_g$) coincides with $\mathbb{M}_6^+(\mathbb{R})$. One example of such materials is wood, which typically exhibits orthotropy in local cylindrical coordinates: in this case, the unit vectors $\boldsymbol{a}$, $\boldsymbol{b}$ and $\boldsymbol{c}$ defining the three orientations are taken as $\boldsymbol{e}_r(\boldsymbol{x})$, $\boldsymbol{e}_\theta(\boldsymbol{x})$ and $\boldsymbol{e}_z(\boldsymbol{x})$ at point $\boldsymbol{x}$ (see Fig. 1 and Sec. 3.2), and the material appears as triclinic in $\mathfrak{R}_g$.

It is assumed that the mean field $\boldsymbol{x} \mapsto [\underline{C}(\boldsymbol{x})] := \mathbb{E}\{[\boldsymbol{C}(\boldsymbol{x})]\}$ satisfies a uniform coercivity condition. An algebraic decomposition is first introduced in order to normalize the random field (in mean), as well as to ensure a uniform ellipticity condition (as discussed in [17] for scalar-valued random fields; see also [1]). This can be achieved in various ways, by letting [1]

$$[\boldsymbol{C}(\boldsymbol{x})] := \frac{1}{1+\epsilon}[\underline{C}(\boldsymbol{x})]^{1/2}\{\epsilon[I_6] + [\boldsymbol{M}(\boldsymbol{x})]\}[\underline{C}(\boldsymbol{x})]^{1/2}, \quad \forall \boldsymbol{x} \in \Omega \tag{2}$$

for instance, with $\epsilon > 0$ a small arbitrary parameter, or by writing

$$[\boldsymbol{C}(\boldsymbol{x})] := [C_0] + ([\underline{C}(\boldsymbol{x})] - [C_0])^{1/2}\,[\boldsymbol{M}(\boldsymbol{x})]\,([\underline{C}(\boldsymbol{x})] - [C_0])^{1/2}, \quad \forall \boldsymbol{x} \in \Omega \tag{3}$$

where $[C_0]$ is a symmetric positive-definite lower bound (*i.e.* $[C_0] < [\boldsymbol{C}(\boldsymbol{x})]$ almost surely, for all $\boldsymbol{x}$ in Ω), the definition of which may be inferred from micromechanical considerations [18,10,13]. In both cases, the construction involves an auxiliary $\mathbb{M}_6^{\mathrm{sym}}(\mathbb{R})$-valued random field $\{[\boldsymbol{M}(\boldsymbol{x})], \boldsymbol{x} \in \Omega\}$ such that

$$\mathbb{E}\{[\boldsymbol{M}(\boldsymbol{x})]\} = [I_6] \tag{4}$$

Next, $\{[\boldsymbol{M}(\boldsymbol{x})], \boldsymbol{x} \in \Omega\}$ is defined by resorting to a pointwise nonlinear mapping, namely

$$[\boldsymbol{M}(\boldsymbol{x})] := \mathcal{H}(\boldsymbol{\Xi}(\boldsymbol{x}), \boldsymbol{x}) \tag{5}$$

where $\{\boldsymbol{\Xi}(\boldsymbol{x}) = (\Xi_1(\boldsymbol{x}), \ldots, \Xi_n(\boldsymbol{x})), \boldsymbol{x} \in \mathbb{R}^3\}$ is a second-order (meaning that $\mathbb{E}\{\|\boldsymbol{\Xi}(\boldsymbol{x})\|^2\}^{1/2} < +\infty$ for all $\boldsymbol{x}$ in $\mathbb{R}^3$) centered Gaussian random field with values in $\mathbb{R}^n$ and $\mathcal{H}$ is made spatially dependent in order to accommodate potential nonstationary cases. As it will be seen later on, the integer n corresponds to the dimension of the matrix set $\mathbb{M}_6^{\mathrm{sym}}(\mathbb{R})$. The Gaussian field $\{\boldsymbol{\Xi}(\boldsymbol{x}), \boldsymbol{x} \in \mathbb{R}^3\}$ is defined by the normalized correlation function $[R]$ such that

$$[R(\boldsymbol{x}, \boldsymbol{y})] := \mathrm{diag}(R_1(\boldsymbol{x}, \boldsymbol{y}), \ldots, R_n(\boldsymbol{x}, \boldsymbol{y})), \quad \forall (\boldsymbol{x}, \boldsymbol{y}) \in \mathbb{R}^3 \times \mathbb{R}^3 \tag{6}$$

with

$$R_k(\boldsymbol{x}, \boldsymbol{y}) = \mathbb{E}\{\Xi_k(\boldsymbol{x})\,\Xi_k(\boldsymbol{y})\}, \quad \forall (\boldsymbol{x}, \boldsymbol{y}) \in \mathbb{R}^3 \times \mathbb{R}^3, \quad 1 \leqslant k \leqslant n \tag{7}$$

and $[R(\boldsymbol{x}, \boldsymbol{x})] = [I_n]$. Eq. (6) implies that the random fields $\{\Xi_i(\boldsymbol{x}), \boldsymbol{x} \in \mathbb{R}^3\}$ and $\{\Xi_j(\boldsymbol{x}), \boldsymbol{x} \in \mathbb{R}^3\}$, $1 \leqslant i < j \leqslant n$, are statistically independent.

2.2. Construction of mapping $\mathcal{H}$ through entropy maximization

Following [9,10], the random matrix $[\boldsymbol{M}(\boldsymbol{x})]$ ($\boldsymbol{x}$ being fixed) is decomposed onto the second-order representation of the (potentially spatially dependent) deterministic Walpole basis $\mathcal{B}_{\boldsymbol{x}} = \{[E_i(\boldsymbol{x})]\}_{i=1}^n$ (see [19]):

$$[\boldsymbol{M}(\boldsymbol{x})] = \sum_{i=1}^{n} M_i(\boldsymbol{x})[E_i(\boldsymbol{x})] \tag{8}$$

Table 1
Values of n, p and r for selected symmetry classes (reduced parameterizations are used for the tetragonal and trigonal classes).

Symmetry class	n	p	r
Isotropy	2	0	–
Cubic	3	0	–
Transverse isotropy	5	1	2
Tetragonal	6	1	2
Trigonal	6	2	2
Orthotropy	9	1	3
Triclinic	21	1	6

where $\{M_i(\boldsymbol{x}), \boldsymbol{x} \in \Omega\}$, $1 \leqslant i \leqslant n$, are scalar random fields. The random vector $\boldsymbol{M}(\boldsymbol{x}) := (M_1(\boldsymbol{x}), \ldots, M_n(\boldsymbol{x}))$ of coefficients takes its values in the set $\mathcal{S}_{\boldsymbol{x}}$ in $\mathbb{R}^n$ such that

$$\mathcal{S}_{\boldsymbol{x}} := \{\boldsymbol{m} \in \mathbb{R}^n \mid \sum_{i=1}^{n} m_i [E_i(\boldsymbol{x})] \in \mathbb{M}_6^+\} \tag{9}$$

The decomposition defined by Eq. (8) can be written by using the symbolic representation

$$[\boldsymbol{M}(\boldsymbol{x})] := \left\{[\boldsymbol{N}^{(1)}(\boldsymbol{x})], \ldots, [\boldsymbol{N}^{(p)}(\boldsymbol{x})], M_{N+1}(\boldsymbol{x}), \ldots, M_n(\boldsymbol{x})\right\} \tag{10}$$

where $\{[\boldsymbol{N}^{(i)}(\boldsymbol{x})]\}_{i=1}^{p}$ is a set of p random matrices with values in $\mathbb{M}_r^+$, the entries of which are made up of the first $N := p \times r(r+1)/2$ coordinates of $[\boldsymbol{M}(\boldsymbol{x})]$ onto $\mathcal{B}_{\boldsymbol{x}}$ (see Eq. (8)). The values of n, p and r are listed in Table 1 for all symmetry classes of practical interest (monoclinic systems are not explicitly considered hereinafter, due to their restricted applicability).

Note that for the isotropic and cubic symmetries, $p = 0$ and the decomposition does not involve any random matrix. For a given symmetry class, the identity matrix $[I_6]$ is given by

$$[I_6] = \{\underbrace{[I_r], \ldots, [I_r]}_{p \text{ times}}, \underbrace{1, \ldots, 1}_{(n-N) \text{ times}}\} \tag{11}$$

The symbolic representation defined by Eq. (10) reflects the particular underlying structure of the tensor (sub)algebras, and allows for simple calculations within $\mathbb{M}_6^{\mathrm{sym}}(\mathbb{R})$. It can be shown, for instance, that

$$[\boldsymbol{M}(\boldsymbol{x})]^{-1} = \left\{[\boldsymbol{N}^{(1)}(\boldsymbol{x})]^{-1}, \ldots, [\boldsymbol{N}^{(p)}(\boldsymbol{x})]^{-1}, M_{N+1}(\boldsymbol{x})^{-1}, \ldots, M_n(\boldsymbol{x})^{-1}\right\} \tag{12}$$

and the following property

$$\Psi([\boldsymbol{M}(\boldsymbol{x})]) = \left\{\Psi([\boldsymbol{N}^{(1)}(\boldsymbol{x})]), \ldots, \Psi([\boldsymbol{N}^{(p)}(\boldsymbol{x})]), \Psi(M_{N+1}(\boldsymbol{x})), \ldots, \Psi(M_n(\boldsymbol{x}))\right\} \tag{13}$$

holds for any deterministic polynomial transformation Ψ. Furthermore, $[\boldsymbol{M}(\boldsymbol{x})]$ is positive-definite almost surely if and only if all the random matrices $\{[\boldsymbol{N}^{(i)}(\boldsymbol{x})]\}_{i=1}^{p}$ and random variables $\{M_i(\boldsymbol{x})\}_{i=N+1}^{n}$ are respectively positive-definite and positive almost surely. It should be noticed that while $[\boldsymbol{M}(\boldsymbol{x})]$ takes its values in $\mathbb{M}$, all the random matrices take their values, in contrast, in $\mathbb{M}_r^+(\mathbb{R})$. These properties will be used in the sequel in order to construct the probabilistic model on the elementary elements of the symbolic representation, as well as to derive closed-form expressions for some model parameters. For example, one has $n = 5$, $p = 1$ and $r = 2$ in the case of a transversely isotropic material, and Eq. (10) reads as

$$[\boldsymbol{M}(\boldsymbol{x})] = \left\{\begin{bmatrix} M_1(\boldsymbol{x}) & M_3(\boldsymbol{x}) \\ M_3(\boldsymbol{x}) & M_2(\boldsymbol{x}) \end{bmatrix}, M_4(\boldsymbol{x}), M_5(\boldsymbol{x})\right\} \tag{14}$$

The mapping $\mathcal{H}$ is then constructed by imposing that the family of first-order marginal probability density functions of $\{[\boldsymbol{M}(\boldsymbol{x})], \boldsymbol{x} \in \Omega\}$ coincides with a target family obtained through an entropy maximization [2,9,10]. The latter is performed by maximizing Shannon's differential entropy

$$S(p) = -\int_{\mathbb{M}_6^+(\mathbb{R})} p([M]) \log(p([M]))\, \mathrm{d}[M] \tag{15}$$

where p is a probability density function and $\mathrm{d}[M] = 2^{15/2} \prod_{i \leqslant j} \mathrm{d}[M]_{ij}$ is the measure in $\mathbb{M}_6^{\mathrm{S}}(\mathbb{R})$ [20] (with $\mathrm{d}[M]_{ij}$ the Lebesgue measure in $\mathbb{R}$), under the constraints

$$\mathbb{E}\{[\boldsymbol{M}(\boldsymbol{x})]\} = [I_6] \tag{16}$$

and

$$\mathbb{E}\{\log(\det([\boldsymbol{M}(\boldsymbol{x})]))\} = \varsigma(\boldsymbol{x}), \quad |\varsigma(\boldsymbol{x})| < +\infty \tag{17}$$

Eq. (16) follows from the normalization in mean, while Eq. (17), together with the proper regularization near the origin, ensures the well-posedness of the associated stochastic boundary value problem (see [2] for proofs). In [9,10], the above constraints were handled by resorting to an exponential mapping. One advantage of this approach was to relax the constraints related to sampling over $\mathcal{S}_{\boldsymbol{x}}$, hence allowing for the recourse to generation algorithms based on stochastic differential equations. An alternative construction can be pursued as follows. First, note that Eqs. (10) and (16) readily imply that

$$\mathbb{E}\{[\boldsymbol{N}^{(i)}(\boldsymbol{x})]\} = [I_r], \quad 1 \leqslant i \leqslant p \tag{18}$$

and

$$\mathbb{E}\{M_k(\boldsymbol{x})\} = 1, \quad N+1 \leqslant k \leqslant n \tag{19}$$

Then, applying Jensen's inequality yields

$$\mathbb{E}\left\{\log\left(\det\left(\sum_{i=1}^{n} M_i(\boldsymbol{x})[E_i(\boldsymbol{x})]\right)\right)\right\} \leqslant \log(\det([I_6])) = 0 \tag{20}$$

where the concavity of the mapping $[X] \mapsto \log(\det([X]))$ for $[X] \in \mathbb{M}_6^+(\mathbb{R})$ (see, *e.g.*, [21]) was used. Upon using the aforementioned symbolic decomposition, one has

$$\log(\det(\sum_{i=1}^{n} M_i(\boldsymbol{x})[E^{(i)}(\boldsymbol{x})])) = \sum_{j=1}^{p} \alpha_j \log\left(\det\left([\boldsymbol{N}^{(j)}(\boldsymbol{x})]\right)\right) + \sum_{k=N+1}^{n} \beta_{k-N} \log(M_k(\boldsymbol{x})) \tag{21}$$

where $\{\alpha_j\}_{j=1}^{p}$ and $\{\beta_k\}_{k=1}^{n-N}$ are two sets of positive integers (see Appendix A for the proof). As mentioned previously, the first sum in the right-hand side of the equation above vanishes for the isotropic and cubic classes (for which $p = 0$). On the other hand, the second sum disappears for the triclinic case ($p = 1$). Applying Jensen's inequality again, it is seen that

$$\mathbb{E}\left\{\log\left(\det\left([\boldsymbol{N}^{(j)}(\boldsymbol{x})]\right)\right)\right\} \leqslant 0, \quad 1 \leqslant j \leqslant p \tag{22}$$

and

$$\mathbb{E}\{\log(M_k(\boldsymbol{x}))\} \leqslant 0, \quad N+1 \leqslant k \leqslant n \tag{23}$$

Therefore, Eq. (17) can be equivalently written as

$$\mathbb{E}\left\{\log\left(\det\left([\boldsymbol{N}^{(j)}(\boldsymbol{x})]\right)\right)\right\} = \nu_j^m(\boldsymbol{x}), \quad |\nu_j^m(\boldsymbol{x})| < +\infty, \quad 1 \leqslant j \leqslant p \tag{24}$$

and

$$\mathbb{E}\{\log(M_k(\boldsymbol{x}))\} = \nu_k^s(\boldsymbol{x}), \quad |\nu_k^s(\boldsymbol{x})| < +\infty, \quad N+1 \leqslant k \leqslant n \tag{25}$$

It follows that the constraints on the random matrices $\{[\boldsymbol{N}^{(j)}(\boldsymbol{x})]\}_{j=1}^{p}$ and the remaining coordinates $\{M_k(\boldsymbol{x})\}_{k=N+1}^{n}$ can be decoupled and considered separately in the stochastic modeling steps. These steps are discussed in the next two subsections.

2.2.1. Stochastic representation of the matrix-valued random fields ($p \neq 0$)

Let us first consider the modeling of random matrix $[\boldsymbol{N}^{(j)}(\boldsymbol{x})]$, $1 \leqslant j \leqslant p$ (recall that $\boldsymbol{x}$ is purposely fixed here). It was shown in [14] that under the constraints given by Eq. (18) and Eq. (24), the probability density function of $[\boldsymbol{N}^{(j)}(\boldsymbol{x})]$ maximizing the entropy

$$S(p) = -\int_{\mathbb{M}_r^+(\mathbb{R})} p([N]) \log(p([N]))\, \mathrm{d}[N] \tag{26}$$

is given by

$$p_{[\boldsymbol{N}^{(j)}(\boldsymbol{x})]}([N]) = \mathbb{1}_{\mathbb{M}_r^+(\mathbb{R})}([N]) \times c_0 \times (\det([N]))^{\chi_r} \times \exp\left(-\frac{(r+1)}{2\delta^2_{[\boldsymbol{N}^{(j)}(\boldsymbol{x})]}}\mathrm{Tr}([N])\right) \tag{27}$$

where $\delta_{[\boldsymbol{N}^{(j)}(\boldsymbol{x})]}$ is the dispersion parameter of $[\boldsymbol{N}^{(j)}(\boldsymbol{x})]$ (defined by Eq. (1)) and

$$\chi_r := \frac{(r+1)(1-\delta^2_{[\boldsymbol{N}^{(j)}(\boldsymbol{x})]})}{(2\delta^2_{[\boldsymbol{N}^{(j)}(\boldsymbol{x})]})} \tag{28}$$

Additionally, $[\boldsymbol{N}^{(j)}(\boldsymbol{x})]$ admits the decomposition

$$[\boldsymbol{N}^{(j)}(\boldsymbol{x})] = [\boldsymbol{H}^{(j)}(\boldsymbol{x})]^{\mathrm{T}}\,[\boldsymbol{H}^{(j)}(\boldsymbol{x})], \quad \forall\,\boldsymbol{x}\in\Omega \tag{29}$$

where $[\boldsymbol{H}^{(j)}(\boldsymbol{x})]$ is an upper-triangular random matrix, the entries of which can be expressed as [2]

$$[\boldsymbol{H}^{(j)}(\boldsymbol{x})]_{k\ell} = \frac{\delta_{[\boldsymbol{N}^{(j)}(\boldsymbol{x})]}}{\sqrt{r+1}}\,U_{k\ell}^{(j)}(\boldsymbol{x}), \quad 1\leqslant k<\ell\leqslant r \tag{30}$$

and

$$[\boldsymbol{H}^{(j)}(\boldsymbol{x})]_{\ell\ell} = \frac{\delta_{[\boldsymbol{N}^{(j)}(\boldsymbol{x})]}}{\sqrt{r+1}}\sqrt{2\mathfrak{G}^{-1}(\Phi(U_{\ell\ell}^{(j)}(\boldsymbol{x}))|\gamma_{\ell}^{(j)}(\boldsymbol{x}),1)}\,, \quad \ell=1,\ldots,r \tag{31}$$

where $\{U_{k\ell}^{(j)}(\boldsymbol{x})\}_{1\leqslant k\leqslant\ell\leqslant r}$ is a collection of $r(r+1)/2$ independent standard normal random variables, $\mathfrak{G}^{-1}(\cdot|a,b)$ is the inverse cumulative distribution function of the Gamma distribution with parameters $a>0$ and $b>0$, Φ is the cumulative distribution function of the standard normal distribution and $\gamma_{\ell}^{(j)}(\boldsymbol{x})$ is given by

$$\gamma_{\ell}^{(j)}(\boldsymbol{x}) := \frac{r+1}{2\delta^2_{[\boldsymbol{N}^{(j)}(\boldsymbol{x})]}} + \frac{1-\ell}{2} \tag{32}$$

Each random field $\{[\boldsymbol{H}^{(j)}(\boldsymbol{x})],\boldsymbol{x}\in\Omega\}$ is then defined by substituting $\Xi_{\alpha(j,k,\ell)}(\boldsymbol{x})$ for $U_{k\ell}^{(j)}(\boldsymbol{x})$ in Eqs. (30) and (31) for all $\boldsymbol{x}$ in Ω and $1\leqslant k\leqslant\ell\leqslant r$, where $\{\Xi_s(\boldsymbol{x}),\boldsymbol{x}\in\mathbb{R}^3\}$ denotes the s-th (independent) component of the vector-valued random field $\{\boldsymbol{\Xi}(\boldsymbol{x}),\boldsymbol{x}\in\mathbb{R}^3\}$ introduced in Sec. 2.1, and $\alpha(j,k,\ell)$ is the positive integer defined as

$$\alpha(j,k,\ell) := k+\frac{1}{2}\,(r(r+1)(j-1)+\ell(\ell-1)) \tag{33}$$

More explicitly, one has

$$[\boldsymbol{H}^{(j)}(\boldsymbol{x})]_{k\ell} := \frac{\delta_{[\boldsymbol{N}^{(j)}(\boldsymbol{x})]}}{\sqrt{r+1}}\,\Xi_{\alpha(j,k,\ell)}(\boldsymbol{x}), \quad 1\leqslant k<\ell\leqslant r \tag{34}$$

and

$$[\boldsymbol{H}^{(j)}(\boldsymbol{x})]_{\ell\ell} := \frac{\delta_{[\boldsymbol{N}^{(j)}(\boldsymbol{x})]}}{\sqrt{r+1}}\sqrt{2\mathfrak{G}^{-1}(\Phi(\Xi_{\alpha(j,\ell,\ell)}(\boldsymbol{x}))|\gamma_{\ell}^{(j)}(\boldsymbol{x}),1)}, \quad \ell=1,\ldots,r \tag{35}$$

In accordance with Eq. (10), let $\{\boldsymbol{\Xi}(\boldsymbol{x}),\boldsymbol{x}\in\mathbb{R}^3\}$ be formerly decomposed as

$$\{\boldsymbol{\Xi}(\boldsymbol{x}),\boldsymbol{x}\in\mathbb{R}^3\} = \{(\boldsymbol{\Xi}^{(1)}(\boldsymbol{x}),\ldots,\boldsymbol{\Xi}^{(p)}(\boldsymbol{x}),\Xi_{N+1}(\boldsymbol{x}),\ldots,\Xi_n(\boldsymbol{x})),\boldsymbol{x}\in\mathbb{R}^3\} \tag{36}$$

where each random field $\{\boldsymbol{\Xi}^{(j)}(\boldsymbol{x}),\boldsymbol{x}\in\mathbb{R}^3\}$, $1\leqslant j\leqslant p$, is a Gaussian random vector of length $r(r+1)/2$. The above construction then defines a pointwise nonlinear mapping between $\{\boldsymbol{\Xi}^{(j)}(\boldsymbol{x}),\boldsymbol{x}\in\Omega\}$ and $\{[\boldsymbol{N}^{(j)}(\boldsymbol{x})],\boldsymbol{x}\in\Omega\}$, $1\leqslant j\leqslant p$.

2.2.2. Stochastic representation of the scalar-valued random fields

Let us now address the case of the remaining coordinates $\{M_k(\boldsymbol{x})\}_{k=N+1}^{n}$, which are assumed to satisfy constraints given by Eqs. (19) and (25). For these components, applying the principle of maximum entropy (for which the entropy writes

$$S(p) = -\int_{\mathbb{R}_*^+} p(m)\,\log(p(m))\,\mathrm{d}m \tag{37}$$

with $\mathbb{R}_*^+=(0,+\infty)$) shows that each random variable $M_k(\boldsymbol{x})$ ($\boldsymbol{x}$ being fixed) follows a Gamma distribution with parameters $(\delta^{-2}_{M_k(\boldsymbol{x})},\delta^2_{M_k(\boldsymbol{x})})$, namely

$$p_{M_k(\boldsymbol{x})}(m) = \mathbb{1}_{\mathbb{R}_*^+}(m)\times c_0\times m^{\delta^{-2}_{M_k(\boldsymbol{x})}-1}\times\exp\left(-\frac{m}{\delta^2_{M_k(\boldsymbol{x})}}\right) \tag{38}$$

with $\delta_{M_k(\boldsymbol{x})}$ the coefficient of variation of $M_k(\boldsymbol{x})$. As a consequence, each random field $\{M_k(\boldsymbol{x}),\boldsymbol{x}\in\Omega\}$, $N+1\leqslant k\leqslant n$, can be defined through the pointwise mapping:

$$M_k(\boldsymbol{x}) := \mathfrak{G}^{-1}(\Phi(\Xi_k(\boldsymbol{x}))|\delta^{-2}_{M_k(\boldsymbol{x})},\delta^2_{M_k(\boldsymbol{x})}), \quad \forall\boldsymbol{x}\in\Omega \tag{39}$$

Similarly, this construction defines a pointwise mapping between $\{\Xi_k(\boldsymbol{x}),\boldsymbol{x}\in\Omega\}$ and $\{M_k(\boldsymbol{x}),\boldsymbol{x}\in\Omega\}$, $N+1\leqslant k\leqslant n$.

2.2.3. Putting things together

The nonlinear mapping $\mathcal{H}$ is completely defined by substituting Eqs. (34) and (35) into (29), and by plugging the results in (10) (or equivalently, in (8)) taking into account (39). This enables, in particular, a fast and robust sampling of the $\mathbb{M}$-valued stochastic field $\{[\boldsymbol{M}(\boldsymbol{x})], \boldsymbol{x} \in \Omega\}$ (and then, of $\{[\boldsymbol{C}(\boldsymbol{x})], \boldsymbol{x} \in \Omega\}$). A sketch of the associated sampling algorithm is provided below:

(I) Select:
  (i) the symmetry class of interest, and deduce n, p, r and $\mathcal{B}_{\boldsymbol{x}}$ (see Appendix C, as well as [19]),
  (ii) values for the dispersion fields $\{\boldsymbol{x} \mapsto \delta_{[\boldsymbol{N}^{(j)}(\boldsymbol{x})]}\}_{j=1}^{p}$ and $\{\boldsymbol{x} \mapsto \delta_{M_k(\boldsymbol{x})}\}_{k=N+1}^{n}$,
  (iii) a suitable autocorrelation function $[R]$ for the Gaussian field $\{\Xi(\boldsymbol{x}), \boldsymbol{x} \in \Omega\}$.

(II) Perform a Monte Carlo loop:
  (i) generate one realization of the Gaussian fields $\{\Xi_k(\boldsymbol{x}), \boldsymbol{x} \in \Omega\}$, $1 \leqslant k \leqslant n$,
  (ii) if $p \neq 0$ (all symmetry classes, except the isotropic and cubic cases), then for $1 \leqslant j \leqslant p$, deduce the realization of the fields $\{[\boldsymbol{H}^{(j)}(\boldsymbol{x}), \boldsymbol{x} \in \Omega]\}$ using Eqs. (34) and (35) (with Eq. (33)), and compute the realization of the fields $\{[\boldsymbol{N}^{(j)}(\boldsymbol{x}), \boldsymbol{x} \in \Omega]\}$ using Eqs. (29),
  (iii) for $N+1 \leqslant k \leqslant n$, deduce the realization of the fields $\{M_k(\boldsymbol{x}), \boldsymbol{x} \in \Omega\}$ using Eqs. (39),
  (iv) for any $\boldsymbol{x} \in \Omega$, compute the realization of $[\boldsymbol{M}(\boldsymbol{x})]$ using Eq. (8).

It should be noticed here that the choice of the autocorrelation function $(\boldsymbol{x}, \boldsymbol{y}) \mapsto [R(\boldsymbol{x}, \boldsymbol{y})]$ is of paramount importance from a modeling standpoint, since it essentially governs key properties of $\{\Xi(\boldsymbol{x}), \boldsymbol{x} \in \Omega\}$ and then, of $\{[M(\boldsymbol{x})], \boldsymbol{x} \in \Omega\}$. In particular, if $[R]$ is such that the Gaussian random field $\{\Xi(\boldsymbol{x}), \boldsymbol{x} \in \Omega\}$ has continuous sample paths (see [22] for a discussion), then the random field $\{[M(\boldsymbol{x})], \boldsymbol{x} \in \Omega\}$ also has a continuous version.

Finally, the dispersion of the stochastic field $\{[\boldsymbol{M}(\boldsymbol{x})], \boldsymbol{x} \in \Omega\}$ can readily be related to the dispersion parameters of the underlying coordinate random fields. More precisely, it can be shown that

$$\delta^2_{[\boldsymbol{M}(\boldsymbol{x})]} = \frac{1}{6}\left(r \sum_{j=1}^{p} \alpha_j \, \delta^2_{[\boldsymbol{N}^{(j)}(\boldsymbol{x})]} + \sum_{k=N+1}^{n} \beta_{k-N} \, \delta^2_{M_k(\boldsymbol{x})} \right) \tag{40}$$

where $\{\alpha_j\}_{j=1}^{p}$ and $\{\beta_{k-N}\}_{k=N+1}^{n}$ have been introduced in Eq. (21) (see Appendix B for the proof). This relation, which is made explicit for all considered classes in Sec. 3 and Appendix C, allows different levels of statistical fluctuations to be prescribed for separate components.

Remark 2.1. While previous information-theoretic approaches for random fields have involved similar constraints (which are related, in part, to the well-posedness of the stochastic boundary value problem) in the definition of the family of first-order marginal distributions, the proposed framework takes advantage of the structure of the tensor set to properly define the matrix-valued and scalar-valued random fields (defining the matrix-valued random field of elasticity tensor with the target symmetry class) through memoryless transformations. This is notably in contrast with the formulation constructed in [10,11], based on the use of an exponential map, where the sampling strategy requires solving a family of Itô stochastic differential equations (ISDE) indexed in space. The latter method is general and can accommodate arbitrary first-order marginal distributions, but it requires the selection of an appropriate integration scheme [23] and the generation of as many realizations of "n" Gaussian random fields as necessary to reach the stationary solution at every single point of the domain. Although the proposed formulation still necessitates the computation of inverse transformations (such as those appearing in Eqs. (34), (35) and (39)), it allows for substantial computational savings. If $10^{N_{\text{iter}}}$ iterations are necessary to reach the stationary solution with the ISDE approach, the computational cost is then reduced by N_{iter} orders of magnitude with the present method (for a given sampling method of the Gaussian fields). In addition, it turns out to be very easy to implement and does not involve any approximation in the calculation of the Lagrange multipliers, since closed-form expressions can be obtained for these hyperparameters.

Remark 2.2. In the proposed construction, the correlation function of the random field $\{[\boldsymbol{M}(\boldsymbol{x})], \boldsymbol{x} \in \Omega\}$ depends on the nonlinear mapping $\mathcal{H}$ and the correlation function $(\boldsymbol{x}, \boldsymbol{y}) \mapsto [R(\boldsymbol{x}, \boldsymbol{y})]$ defining the underlying Gaussian field $\{\Xi(\boldsymbol{x}), \boldsymbol{x} \in \Omega\}$. The selection of $[R]$ is therefore critical, not only to ensure suitable properties for the Gaussian field (as indicated previously), but also to mimic the features of some potential experiments. In the case this choice generates an error between the simulations and the available experimental data, the correlation kernel may be updated by pursuing the following approach. Let us assume that we are given a set $\{(\boldsymbol{x}, \boldsymbol{y}) \mapsto R_i(\boldsymbol{x}, \boldsymbol{y})\}_{i=1}^{n}$ of normalized correlation functions with appropriate properties: these functions typically correspond to a choice made a priori (with no reliance on data whatsoever). Furthermore, let us assume that the target correlation functions are square-integrable. By Mercer's theorem, one has

$$R_i(\boldsymbol{x}, \boldsymbol{y}) = \sum_{j=1}^{+\infty} \lambda_j^{(i)} \psi_j^{(i)}(\boldsymbol{x}) \psi_j^{(i)}(\boldsymbol{y}), \quad 1 \leqslant i \leqslant n \tag{41}$$

where $\{\lambda_j^{(i)}\}_{j\geqslant 1}$ and $\{\psi_j^{(i)}\}_{j\geqslant 1}$ are the (strictly positive) eigenvalues and eigenfunctions of R_i, defined as the solutions to the Fredholm equation of the second kind

$$\int_{\overline{\Omega}} R_i(\boldsymbol{x},\boldsymbol{y})\psi_j^{(i)}(\boldsymbol{y})\mathrm{d}\boldsymbol{y} = \lambda_j^{(i)}\psi_j^{(i)}(\boldsymbol{x}) \tag{42}$$

Since the functions $\{\psi_j^{(i)}\}_{j\geqslant 1}$ constitute a basis of the Hilbert space $L^2(\overline{\Omega},\mathbb{R})$, each correlation function involved in the model may then be updated and defined, at order $\mathcal{E}_i$, as

$$\widehat{R}_i(\boldsymbol{x},\boldsymbol{y}) := \sum_{j=1}^{\mathcal{E}_i} \widehat{\lambda}_j^{(i)}\psi_j^{(i)}(\boldsymbol{x})\psi_j^{(i)}(\boldsymbol{y}) \tag{43}$$

where $\widehat{R}_i$ is the "new" correlation kernel associated with $\{\Xi_i(\boldsymbol{x}),\boldsymbol{x}\in\Omega\}$ and the strictly positive eigenvalues $\widehat{\lambda}_j^{(i)}$, $1\leqslant j\leqslant \mathcal{E}_i$, are the solutions to an appropriate optimization problem involving some measured quantity of interest (such as a displacement field). In this context, the eigenvalues of the covariance kernel appear as additional hyperparameters. It should be noticed here that updating this kernel substantially increases the size of the identification problem (in contrast to strategies relying on a minimal parametrization of the covariance functions), and that the associated inverse problem may be strongly ill posed.

3. Numerical examples

In order to illustrate some of the capabilities of the model, two examples involving weak symmetries and fields indexed by non-polyhedral geometries in $\mathbb{R}^3$ are provided below. The generation of the underlying Gaussian random fields $\{\Xi_k(\boldsymbol{x}),\boldsymbol{x}\in\Omega\}$, $1\leqslant k\leqslant n$, can be carried out by various methods, including the spectral approach, (iterative) factorization-based methods or filtering techniques (a discussion about these algorithms is beyond the scope of this paper). In this work, this sampling task is performed by having recourse to the stochastic differential equation approach proposed in [24]. Each random field $\{\Xi_k(\boldsymbol{x}),\boldsymbol{x}\in\Omega\}$ is then defined as the solution to a stochastic differential equation and an appropriate Markov approximation is constructed by means of the finite element method. Here, we consider the anisotropic version of the fractional stochastic differential equation (SDE) [25,26], namely

$$\left[\kappa^2(\boldsymbol{x}) - \langle\nabla,[D(\boldsymbol{x})]\nabla\rangle\right]^{\zeta/2}\Xi_k(\boldsymbol{x}) = \mathcal{W}(\boldsymbol{x}), \quad \boldsymbol{x}\in\Omega \tag{44}$$

where $\kappa(\boldsymbol{x})>0$ is a free parameter scaling the correlation of the solution (in practice, the correlation range and $\kappa(\boldsymbol{x})$ present opposite variations), $[D(\boldsymbol{x})]$ is a positive-definite matrix (which is referred to as the diffusion matrix and may depend on k, if need be), $\zeta=\nu+3/2$ with $\nu>0$ (for three-dimensional applications), and $\{\mathcal{W}(\boldsymbol{x}),\boldsymbol{x}\in\Omega\}$ is the normalized Gaussian white noise. The parameter ν controls the smoothness of the solution, and the value $\nu=1/2$ (hence, $\zeta=2$) is selected in the rest of this note. In this case, the fractional differential operator vanishes, and a standard Galerkin method can be used to solve the stochastic differential equation. By computing the weak form of Eq. (44) and using homogeneous Neumann boundary conditions (which consist in imposing a zero normal derivative at the boundary), it can be shown that the Markov approximation of the Gaussian random field takes the form [24]

$$\Xi_k(\boldsymbol{x}) = \sum_{i=1}^{q} W_i\,\varphi_i(\boldsymbol{x}) \tag{45}$$

where $\{\varphi_i\}_{i=1}^q$ is a finite element basis. In this paper, piecewise linear functions are selected for simplicity. Moreover, $W_1,\ldots,W_q$ are weights such that the random vector $\boldsymbol{W}:=(W_1,\ldots,W_q)$ follows the Gaussian distribution with mean $\mathbf{0}$ and covariance matrix $[\mathcal{Q}]^{-1}$, where $[\mathcal{Q}]$ is the (sparse) precision matrix given by

$$[\mathcal{Q}] = ([F]+[G])^{\mathrm{T}}\,[\widehat{F}]^{-1}\,([F]+[G]) \tag{46}$$

In Eq. (46), $[\widehat{F}]$ is the diagonal $(q\times q)$ matrix with entries $[\widehat{F}]_{ii}:=\sum_{j=1}^q[\widetilde{F}]_{ij}$, wherein

$$[\widetilde{F}]_{ij} := \int_{\Omega}\varphi_i(\boldsymbol{x})\,\varphi_j(\boldsymbol{x})\,\mathrm{d}\boldsymbol{x} \tag{47}$$

The $(q\times q)$ matrices $[F]$ and $[G]$, obtained by finite element assembling, are further defined component-wise as

$$[F]_{ij} := \int_{\Omega}\kappa^2(\boldsymbol{x})\,\varphi_i(\boldsymbol{x})\,\varphi_j(\boldsymbol{x})\,\mathrm{d}\boldsymbol{x}, \quad [G]_{ij} := \int_{\Omega}\langle\nabla\varphi_i(\boldsymbol{x}),[D(\boldsymbol{x})]\,\nabla\varphi_j(\boldsymbol{x})\rangle\,\mathrm{d}\boldsymbol{x}, \quad 1\leqslant i,j\leqslant q \tag{48}$$

When the fields $\boldsymbol{x} \mapsto \kappa(\boldsymbol{x})$ and $\boldsymbol{x} \mapsto [D(\boldsymbol{x})]$ are both chosen constant, the solution to the SDE (considered in $\mathbb{R}^3$) is stationary and a closed-form expression of the covariance function can be obtained as (see Appendix D)

$$R_k(\boldsymbol{x}, \boldsymbol{y}) = \frac{1}{8\pi\kappa\sqrt{\det([D])}} \exp\left(-\kappa \|[D]^{-1/2}(\boldsymbol{x}-\boldsymbol{y})\|\right), \quad \forall (\boldsymbol{x}, \boldsymbol{y}) \in \mathbb{R}^3 \times \mathbb{R}^3 \tag{49}$$

from which it is seen that the property

$$\frac{1}{8\pi\kappa\sqrt{\det([D])}} = 1 \tag{50}$$

must hold to ensure a unit variance. If $[D] = \mathrm{diag}(D_1, D_2, D_3)$, with $D_\ell > 0$ for $1 \leqslant \ell \leqslant 3$, then

$$R_k(\boldsymbol{x}, \boldsymbol{y}) = \frac{1}{8\pi\kappa\sqrt{D_1 D_2 D_3}} \exp\left(-\kappa \left(\sum_{\ell=1}^{3} \frac{(x_\ell - y_\ell)^2}{D_\ell}\right)^{1/2}\right) \tag{51}$$

When the correlation is further characterized along one vector of the canonical basis in $\mathbb{R}^3$, say $\boldsymbol{e}_\ell$ ($1 \leqslant \ell \leqslant 3$), then $\boldsymbol{x} = x\,\boldsymbol{e}_\ell$, $\boldsymbol{y} = y\,\boldsymbol{e}_\ell$ and

$$R_k(\boldsymbol{x}, \boldsymbol{y}) = \frac{1}{8\pi\kappa\sqrt{D_1 D_2 D_3}} \exp\left(-\frac{\kappa}{\sqrt{D_\ell}}|x_\ell - y_\ell|\right) \tag{52}$$

which shows that

$$L_\ell := \frac{\sqrt{D_\ell}}{\kappa} \tag{53}$$

may be interpreted, under the above assumptions, as the spatial correlation length (in the Cartesian coordinate system) along $\boldsymbol{e}_\ell$, with $\kappa = (8\pi L_1 L_2 L_3)^{-1/4}$. In addition, Eq. (53) shows the roles played by D_ℓ and κ, and can be used in order to properly discretize the solution over Ω. In this work, the mesh size is determined through a convergence analysis, using a L^2 metric with the covariance function estimated on refined meshes.

For spatially dependent coefficients, the covariance function inherited by the solution $\{\Xi_k(\boldsymbol{x}), \boldsymbol{x} \in \Omega\}$ (which is not stationary) must be characterized through computational experiments (although some features, such as the anisotropy of the induced correlation structure, can be inferred from κ and the topological structure of $[D]$). Illustrative two-dimensional examples can be found in [25,26] for both stationary and nonstationary cases. Otherwise stated, the coefficient of variation of all the random matrices and random variables is set to $\delta = 0.2$.

Remark 3.1. It should be noticed at this point that the solution $\{\Xi_k(\boldsymbol{x}), \boldsymbol{x} \in \Omega\}$ may suffer from boundary effects, as reported in [24]. These boundary effects, which can be circumvented in part by embedding Ω in a larger domain, raise inappropriate fluctuations in variance, so that the property $[R(\boldsymbol{x}, \boldsymbol{x})] = [I_n]$ may not be satisfied exactly in numerical experiments. If the estimated variance field is either heterogeneous over Ω or not equal to one (or both), a proper scaling of the Gaussian field (in variance) must then be performed in a postprocessing step.

Remark 3.2. From the perspective of uncertainty propagation, one may have recourse to a sampling-based solver or to a classical spectral approach. The latter strategy can readily be formulated by considering Karhunen–Loève expansions of the underlying Gaussian fields $\{\Xi_k(\boldsymbol{x}), \boldsymbol{x} \in \Omega\}$, $1 \leqslant k \leqslant n$, and by using polynomial chaos expansions of quantities of interest in terms of the retained reduced coordinates for all the aforementioned Gaussian random fields.

3.1. Application to spherical transverse isotropy

In this first example, we consider the case of spherical transverse isotropy. This implies that for any $\boldsymbol{x} \in \Omega$, the elasticity tensor exhibits transverse isotropy with respect to the unit normal $\boldsymbol{n}(\boldsymbol{x}) := \boldsymbol{e}_r(\boldsymbol{x})$, with $\boldsymbol{e}_r(\boldsymbol{x})$ the radial basis vector at point $\boldsymbol{x}$. This model was notably shown to be relevant to the modeling of random interphase properties in nanocomposites with spherical fillers [27], for example.

Let $[P(\boldsymbol{x})]$ and $[Q(\boldsymbol{x})]$ be the second-order tensors defined as

$$[P(\boldsymbol{x})] := \boldsymbol{n}(\boldsymbol{x}) \otimes \boldsymbol{n}(\boldsymbol{x}), \quad [Q(\boldsymbol{x})] := [I_3] - [P(\boldsymbol{x})] \tag{54}$$

The local tensor basis is then defined by the second-order tensor representation of the following tensor basis [19]:

$$\begin{aligned}
&[\![E_1(\boldsymbol{x})]\!] := [P(\boldsymbol{x})] \otimes [P(\boldsymbol{x})], \quad [\![E_2(\boldsymbol{x})]\!] := ([Q(\boldsymbol{x})] \otimes [Q(\boldsymbol{x})])/2 \\
&[\![E_3(\boldsymbol{x})]\!] := ([P(\boldsymbol{x})] \otimes [Q(\boldsymbol{x})] + [Q(\boldsymbol{x})] \otimes [P(\boldsymbol{x})])/\sqrt{2} \\
&[\![E_4(\boldsymbol{x})]\!] := [Q(\boldsymbol{x})] \boxtimes [Q(\boldsymbol{x})] - ([Q(\boldsymbol{x})] \otimes [Q(\boldsymbol{x})])/2 \\
&[\![E_5(\boldsymbol{x})]\!] := [P(\boldsymbol{x})] \boxtimes [Q(\boldsymbol{x})] + [Q(\boldsymbol{x})] \boxtimes [P(\boldsymbol{x})]
\end{aligned} \tag{55}$$

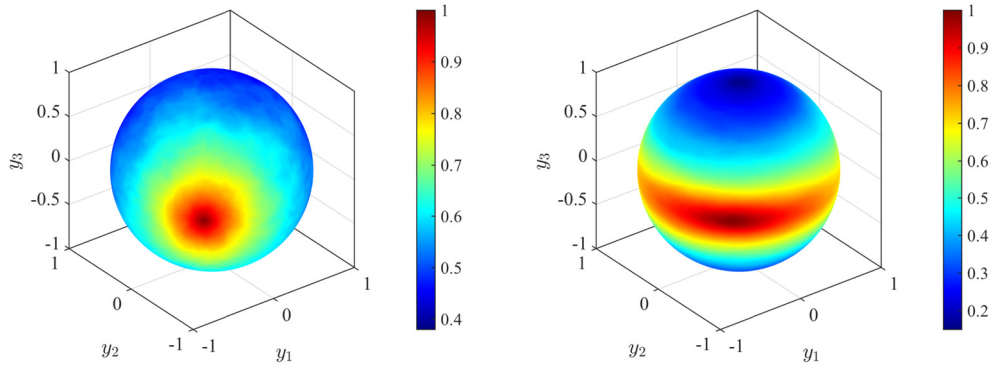

Fig. 2. The left panel displays the graph of the correlation function $\boldsymbol{y} \mapsto R_1(\boldsymbol{x}_0, \boldsymbol{y})$, estimated with 1,000 independent realizations for $\kappa(\boldsymbol{x}) = 2$ and $\lambda_\theta = 0$ ($[D(\boldsymbol{x})] = [I_3]$). The right panel displays the estimated correlation function for $\kappa(\boldsymbol{x}) = 4$ and $\lambda_\theta = 50$, which corresponds to a strongly anisotropic correlation structure. The reference point $\boldsymbol{x}_0$ is arbitrarily chosen on the outer surface of the sphere.

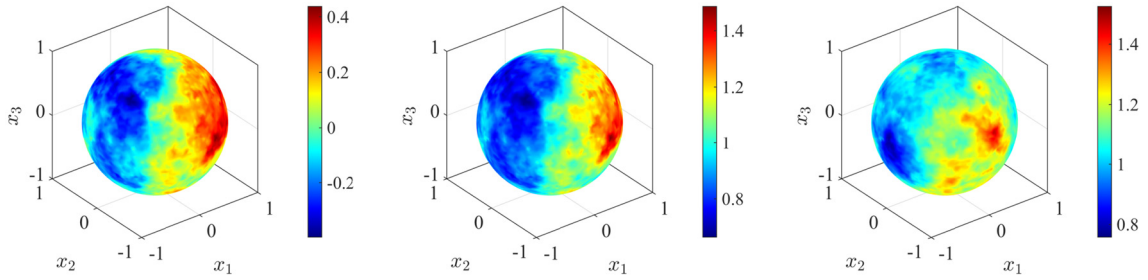

Fig. 3. Illustrative results for $\kappa(\boldsymbol{x}) = 2$ and $\lambda_\theta = 0$. One realization of $\{\Xi_1(\boldsymbol{x}), \boldsymbol{x} \in \Omega\}$ and the associated realizations of $\{M_1(\boldsymbol{x}), \boldsymbol{x} \in \Omega\}$ and $\{[M(\boldsymbol{x})]_{11}, \boldsymbol{x} \in \Omega\}$ are shown in the left, middle and right panels, respectively.

The elasticity field can then be decomposed as

$$[\boldsymbol{M}(\boldsymbol{x})] = \sum_{i=1}^{5} M_i(\boldsymbol{x})\,[E_i(\boldsymbol{x})] = \left\{ \begin{bmatrix} M_1(\boldsymbol{x}) & M_3(\boldsymbol{x}) \\ M_3(\boldsymbol{x}) & M_2(\boldsymbol{x}) \end{bmatrix}, M_4(\boldsymbol{x}), M_5(\boldsymbol{x}) \right\} \tag{56}$$

so that

$$[\boldsymbol{N}^{(1)}(\boldsymbol{x})] = \begin{bmatrix} M_1(\boldsymbol{x}) & M_3(\boldsymbol{x}) \\ M_3(\boldsymbol{x}) & M_2(\boldsymbol{x}) \end{bmatrix} \tag{57}$$

Furthermore, it can be shown that

$$\delta_{[\boldsymbol{M}(\boldsymbol{x})]} = \left\{ \frac{1}{3} \left(\delta^2_{[\boldsymbol{N}^{(1)}(\boldsymbol{x})]} + \delta^2_{M_4(\boldsymbol{x})} + \delta^2_{M_5(\boldsymbol{x})} \right) \right\}^{1/2} \tag{58}$$

We consider sampling inside the unit sphere $\Omega = \{\boldsymbol{x} \in \mathbb{R}^3, \|\boldsymbol{x}\| \leqslant 1\}$, and the field of diffusion tensor in Eq. (44) is taken, for illustration purposes, as

$$[D(\boldsymbol{x})] := [I_3] + \lambda_\theta\, \boldsymbol{e}_\theta(\boldsymbol{x}) \otimes \boldsymbol{e}_\theta(\boldsymbol{x}), \tag{59}$$

where the parameter $\lambda_\theta \geqslant 0$ controls the correlation range along $\boldsymbol{e}_\theta$. From a computational standpoint, the Markov approximation is constructed with $q = 23,623$ nodes. Examples of covariance kernels obtained for two values of the diffusion tensor are shown in Fig. 2. More specifically, the left panel displays an isotropic kernel, while the right panel shows a strongly anisotropic covariance structure where the correlation along $\boldsymbol{e}_\theta$ is more pronounced.

One realization of the first Gaussian random field $\{\Xi_1(\boldsymbol{x}), \boldsymbol{x} \in \Omega\}$ and the associated realizations of the first component $\{M_1(\boldsymbol{x}), \boldsymbol{x} \in \Omega\}$ and $\{[M(\boldsymbol{x})]_{11}, \boldsymbol{x} \in \Omega\}$ are shown for the isotropic case in Fig. 3, while similar results for the anisotropic kernel are depicted in Fig. 4.

A comparison between these figures shows that the diffusion $\boldsymbol{x} \mapsto [D(\boldsymbol{x})]$ strongly affects the local geometry of the elasticity field. From a modeling standpoint, the field of diffusion tensor is a key parameter that may be appropriately defined in order to reproduce morphological features raised by fine scale information (such as the local orientation of polymer chains or fibers, for instance). Finally, an illustration with increasing levels of fluctuation is shown for the scalar random field $\{M_4(\boldsymbol{x}), \boldsymbol{x} \in \Omega\}$ in Fig. 5 (the same realization of the Gaussian field $\{\boldsymbol{\Xi}(\boldsymbol{x}), \boldsymbol{x} \in \Omega\}$ was used for the three subfigures).

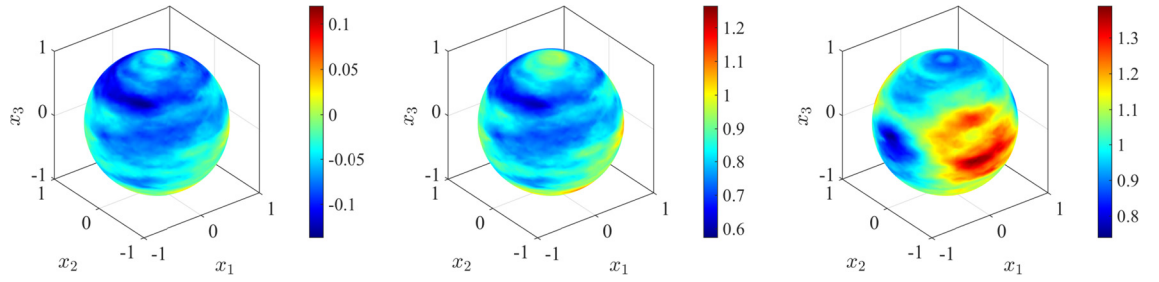

Fig. 4. Illustrative results for $\kappa(\boldsymbol{x}) = 4$ and $\lambda_\theta = 50$. One realization of $\{\Xi_1(\boldsymbol{x}), \boldsymbol{x} \in \Omega\}$ and the associated realizations of $\{M_1(\boldsymbol{x}), \boldsymbol{x} \in \Omega\}$ and $\{[M(\boldsymbol{x})]_{11}, \boldsymbol{x} \in \Omega\}$ are shown in the left, middle and right panels, respectively.

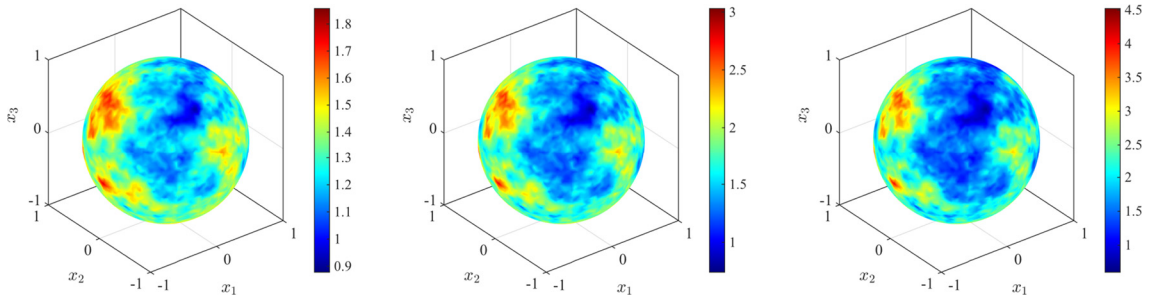

Fig. 5. Illustrative results for $\kappa(\boldsymbol{x}) = 2$ and $\lambda_\theta = 0$. One realization of $\{M_4(\boldsymbol{x}), \boldsymbol{x} \in \Omega\}$ is shown for $\delta = 0.2$ (left), $\delta = 0.4$ (middle) and $\delta = 0.6$ (right), respectively.

3.2. Application to cylindrical (or polar) orthotropy

In this second application, we consider the case of cylindrical orthotropy, with

$$\Omega := \{\boldsymbol{x} \in \mathbb{R}^3, x_1^2 + x_2^2 \leqslant 1, 0 \leqslant x_3 \leqslant 3\}$$

The material is then assumed to exhibit local orthotropy at point $\boldsymbol{x}$, where the crystallographic directions are defined by the unit mutually orthogonal vectors $\boldsymbol{a}(\boldsymbol{x})$, $\boldsymbol{b}(\boldsymbol{x})$ and $\boldsymbol{c}(\boldsymbol{x})$. This field of orientation vectors may be chosen as constant and coincident with the global coordinate system $\mathfrak{R}_g$ to model orthotropic composite laminates, or spatially dependent to model symmetries in the local coordinate system $\mathfrak{R}_\ell$. Here, we address the second situation and define $\boldsymbol{a}(\boldsymbol{x}) := \boldsymbol{e}_r(\boldsymbol{x})$, $\boldsymbol{b}(\boldsymbol{x}) := \boldsymbol{e}_\theta(\boldsymbol{x})$ and $\boldsymbol{c}(\boldsymbol{x}) := \boldsymbol{e}_z(\boldsymbol{x})$, where $\mathfrak{R}_\ell = (\boldsymbol{x}, \boldsymbol{e}_r(\boldsymbol{x}), \boldsymbol{e}_\theta(\boldsymbol{x}), \boldsymbol{e}_z(\boldsymbol{x}))$ denotes the local cylindrical coordinate system at point $\boldsymbol{x}$. This model is, in particular, relevant to the modeling of spatially dependent wood properties. The associated tensor basis is given by [19]:

$$\begin{aligned}
&[\![E_1(\boldsymbol{x})]\!] := \boldsymbol{a}\otimes\boldsymbol{a}\otimes\boldsymbol{a}\otimes\boldsymbol{a}, \quad [\![E_2(\boldsymbol{x})]\!] := \boldsymbol{b}\otimes\boldsymbol{b}\otimes\boldsymbol{b}\otimes\boldsymbol{b}, \quad [\![E_3(\boldsymbol{x})]\!] := \boldsymbol{c}\otimes\boldsymbol{c}\otimes\boldsymbol{c}\otimes\boldsymbol{c} \\
&[\![E_4(\boldsymbol{x})]\!] := \boldsymbol{a}\otimes\boldsymbol{a}\otimes\boldsymbol{b}\otimes\boldsymbol{b} + \boldsymbol{b}\otimes\boldsymbol{b}\otimes\boldsymbol{a}\otimes\boldsymbol{a}, \quad [\![E_5(\boldsymbol{x})]\!] := \boldsymbol{b}\otimes\boldsymbol{b}\otimes\boldsymbol{c}\otimes\boldsymbol{c} + \boldsymbol{c}\otimes\boldsymbol{c}\otimes\boldsymbol{b}\otimes\boldsymbol{b} \\
&[\![E_6(\boldsymbol{x})]\!] := \boldsymbol{a}\otimes\boldsymbol{a}\otimes\boldsymbol{c}\otimes\boldsymbol{c} + \boldsymbol{c}\otimes\boldsymbol{c}\otimes\boldsymbol{a}\otimes\boldsymbol{a}, \quad [\![E_7(\boldsymbol{x})]\!] := (\boldsymbol{a}\otimes\boldsymbol{b} + \boldsymbol{b}\otimes\boldsymbol{a})\otimes(\boldsymbol{a}\otimes\boldsymbol{b} + \boldsymbol{b}\otimes\boldsymbol{a})/2 \\
&[\![E_8(\boldsymbol{x})]\!] := (\boldsymbol{b}\otimes\boldsymbol{c} + \boldsymbol{c}\otimes\boldsymbol{b})\otimes(\boldsymbol{b}\otimes\boldsymbol{c} + \boldsymbol{c}\otimes\boldsymbol{b})/2, \quad [\![E_9(\boldsymbol{x})]\!] := (\boldsymbol{a}\otimes\boldsymbol{c} + \boldsymbol{c}\otimes\boldsymbol{a})\otimes(\boldsymbol{a}\otimes\boldsymbol{c} + \boldsymbol{c}\otimes\boldsymbol{a})/2
\end{aligned} \tag{60}$$

where the spatial dependence of the quantities in the right-hand side is not explicitly stated for notational convenience. The random field of elasticity tensor is written as

$$[\boldsymbol{M}(\boldsymbol{x})] = \sum_{i=1}^{9} M_i(\boldsymbol{x})\,[E_i(\boldsymbol{x})] = \left\{ \begin{bmatrix} M_1(\boldsymbol{x}) & M_4(\boldsymbol{x}) & M_6(\boldsymbol{x}) \\ M_4(\boldsymbol{x}) & M_2(\boldsymbol{x}) & M_5(\boldsymbol{x}) \\ M_5(\boldsymbol{x}) & M_6(\boldsymbol{x}) & M_3(\boldsymbol{x}) \end{bmatrix}, M_7(\boldsymbol{x}), M_8(\boldsymbol{x}), M_9(\boldsymbol{x}) \right\} \tag{61}$$

Hence, one has

$$[\boldsymbol{N}^{(1)}(\boldsymbol{x})] = \begin{bmatrix} M_1(\boldsymbol{x}) & M_4(\boldsymbol{x}) & M_6(\boldsymbol{x}) \\ M_4(\boldsymbol{x}) & M_2(\boldsymbol{x}) & M_5(\boldsymbol{x}) \\ M_5(\boldsymbol{x}) & M_6(\boldsymbol{x}) & M_3(\boldsymbol{x}) \end{bmatrix} \tag{62}$$

and the dispersion parameter $\delta_{[\boldsymbol{M}(\boldsymbol{x})]}$ is found to be such that

$$\delta_{[\boldsymbol{M}(\boldsymbol{x})]} = \left\{ \frac{1}{6} \left(3\delta^2_{[\boldsymbol{N}^{(1)}(\boldsymbol{x})]} + \delta^2_{M_7(\boldsymbol{x})} + \delta^2_{M_8(\boldsymbol{x})} + \delta^2_{M_9(\boldsymbol{x})} \right) \right\}^{1/2} \tag{63}$$

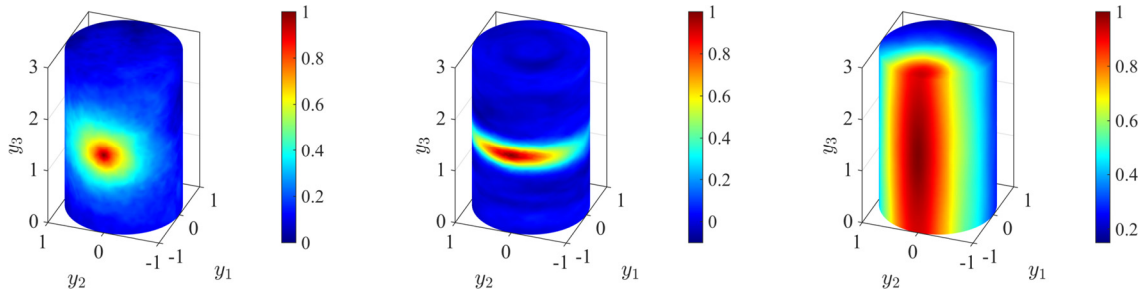

Fig. 6. This figure shows the graph of the correlation function $\boldsymbol{y} \mapsto R_1(\boldsymbol{x}_0, \boldsymbol{y})$, estimated with 1,000 independent realizations, for $(\kappa(\boldsymbol{x}), \lambda_\theta, \lambda_z) = (2, 0, 0)$ (left panel), $(10, 50, 0.1)$ (middle panel) and $(2, 0, 50)$. The reference point $\boldsymbol{x}_0$ is arbitrarily chosen on the outer surface of the cylinder.

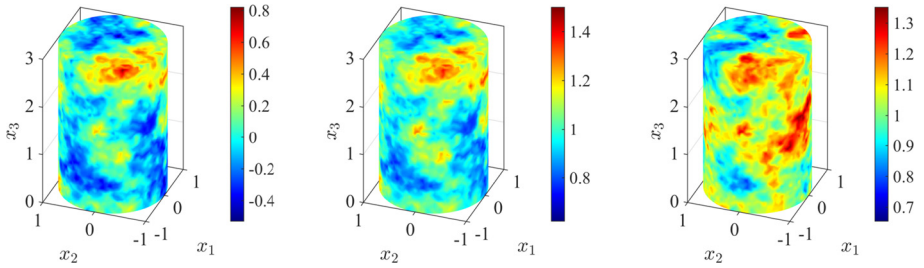

Fig. 7. Illustrative results for $\kappa(\boldsymbol{x}) = 2$ and $\lambda_\theta = \lambda_z = 0$. One realization of $\{\Xi_1(\boldsymbol{x}), \boldsymbol{x} \in \Omega\}$ and the associated realizations of $\{M_1(\boldsymbol{x}), \boldsymbol{x} \in \Omega\}$ and $\{[M(\boldsymbol{x})]_{11}, \boldsymbol{x} \in \Omega\}$ are shown in the left, middle and right panels, respectively.

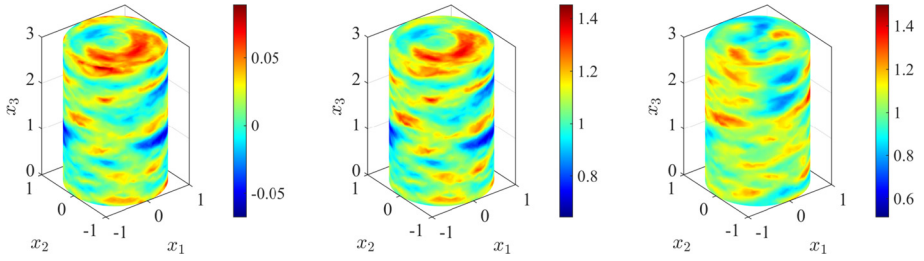

Fig. 8. Illustrative results for $\kappa(\boldsymbol{x}) = 10$, $\lambda_\theta = 50$ and $\lambda_z = 0.1$. One realization of $\{\Xi_1(\boldsymbol{x}), \boldsymbol{x} \in \Omega\}$ and the associated realizations of $\{M_1(\boldsymbol{x}), \boldsymbol{x} \in \Omega\}$ and $\{[M(\boldsymbol{x})]_{11}, \boldsymbol{x} \in \Omega\}$ are shown in the left, middle and right panels, respectively.

The diffusion tensor in Eq. (44) is chosen as

$$[D(\boldsymbol{x})] := [I_3] + \lambda_\theta \, \boldsymbol{e}_\theta(\boldsymbol{x}) \otimes \boldsymbol{e}_\theta(\boldsymbol{x}) + \lambda_z \, \boldsymbol{e}_z(\boldsymbol{x}) \otimes \boldsymbol{e}_z(\boldsymbol{x}) \tag{64}$$

where the parameters $\lambda_\theta \geqslant 0$ and $\lambda_z \geqslant 0$ can be adjusted in order to target some correlation ranges along the associated directions. The Markov approximation is constructed with $q = 16{,}460$. We consider an isotropic covariance kernel (defined with $\lambda_\theta = \lambda_z = 0$), as well as two anisotropic cases where a predominant correlation is locally imposed along $\boldsymbol{e}_\theta$ or $\boldsymbol{e}_z$ as depicted in Fig. 6. One realization of the random field $\{\Xi_1(\boldsymbol{x}), \boldsymbol{x} \in \Omega\}$ and the associated realizations of $\{M_1(\boldsymbol{x}), \boldsymbol{x} \in \Omega\}$ and $\{[M(\boldsymbol{x})]_{11}, \boldsymbol{x} \in \Omega\}$ are shown for the isotropic case in Fig. 7. As expected, it is seen that the realizations do not exhibit any noticeable feature in terms of orientation. Similar results for the two anisotropic configurations are shown in Figs. 8 and 9. In contrast to the isotropic case, it is observed that the realizations obtained with anisotropic kernels can exhibit specific features that may be found representative of subscale details, such as local fiber orientation.

Since the covariance kernel $[R]$ inherited from the choices of κ and $[D]$ is unknown *a priori* for spatially dependent coefficients, we next investigate below, through numerical experiments, the shape of the covariance kernel $(\boldsymbol{x}, \boldsymbol{y}) \mapsto R_1(\boldsymbol{x}, \boldsymbol{y})$. For this purpose, we consider three configurations related to directions of interest, namely:

- the radial direction, for which we select $\boldsymbol{x} = (0, 0, 0)$, $\boldsymbol{y} = (u, 0, 0)$ or $(0, u, 0)$ (with $u \in [-1, 1]$), and let $R_1(\boldsymbol{x}, \boldsymbol{y}) =: \rho_1(u)$;
- the orthoradial direction, which is explored using $\boldsymbol{x} = (r_i, 0, 0)$ and $\boldsymbol{y} = (r_i \cos\theta, r_i \sin\theta, 0)$, with $r_i \in \{0.5, 0.75, 1\}$ and $\theta \in [-\pi, \pi]$; here, we let $R_1(\boldsymbol{x}, \boldsymbol{y}) =: \rho_1(r_i\theta)$, where $r_i\theta$ measures the arc length at $r = r_i$;
- the longitudinal direction, where $\boldsymbol{x} = (u, v, 1.5)$, $\boldsymbol{y} = (u, v, z)$, $u \in \{-1, 0, 1\}$, $v \in \{-1, 0, 1\}$ and $z = [1, 2]$; we then define $R_1(\boldsymbol{x}, \boldsymbol{y}) =: \rho_1(z)$.

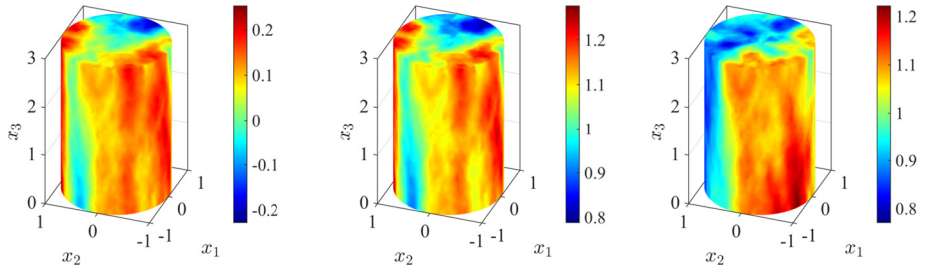

Fig. 9. Illustrative results for $\kappa(\boldsymbol{x}) = 2$, $\lambda_\theta = 0$ and $\lambda_z = 50$. One realization of $\{\Xi_1(\boldsymbol{x}), \boldsymbol{x} \in \Omega\}$ and the associated realizations of $\{M_1(\boldsymbol{x}), \boldsymbol{x} \in \Omega\}$ and $\{[M(\boldsymbol{x})]_{11}, \boldsymbol{x} \in \Omega\}$ are shown in the left, middle and right panels, respectively.

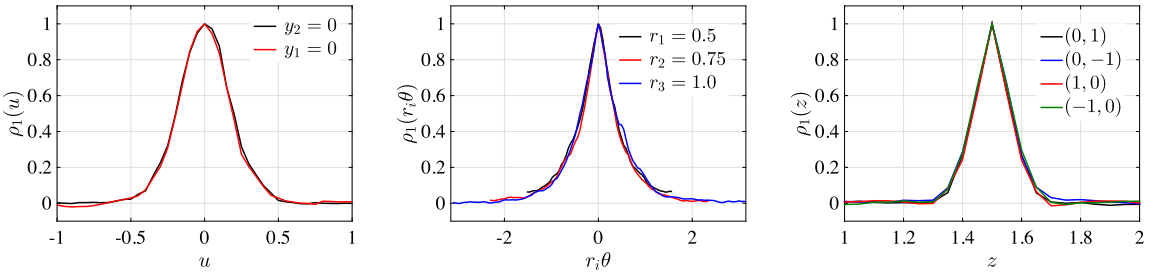

Fig. 10. illustrative results for $\kappa(\boldsymbol{x}) = 20$, $\lambda_\theta = 50$ and $\lambda_z = 0.1$. These figures show the estimated covariance kernels in the selected radial, orthoradial and longitudinal directions. In the right panel, the configurations correspond to values of u and v.

The covariance functions estimated with 20,000 independent realizations are shown for these three configurations in Fig. 10. It can be observed in this figure that the covariance function (expressed in appropriate coordinates) exhibits some invariance properties along preferred directions. These properties are induced by the particular definition of $[D]$, which is chosen in accordance with the geometrical symmetries in this application. While this may suggest stationarity, it is worthwhile to recall that, in the present case, the solution is not stationary (for the translation in $\mathbb{R}^3$).

4. Conclusion

In this Note, we have presented a unified approach to the modeling and simulation of (non-Gaussian) random fields of elasticity tensors. The information-theoretic stochastic representation builds upon the so-called Walpole tensor decomposition, which allows the probabilistic model to be constructed using independent matrix-valued and scalar-valued random fields. In contrast to alternative approaches proposed elsewhere, the model can be sampled through a memoryless transformation, hence providing substantial computational savings. Two applications involving weak symmetries and spherical and cylindrical geometries are finally given in order to exemplify some modeling capabilities of the framework. In particular, it is shown that an appropriate parametrization of the underlying Gaussian fields (through the diffusion field) allows specific features (such as those related to subscale details, including morphological anisotropy) to be prescribed on the sample paths of the random field of elasticity tensor.

Appendix A. Proof of Eq. (21)

Invoking the symbolic representation, one has

$$\begin{aligned}\log(\det([\boldsymbol{M}(\boldsymbol{x})])) &= \mathrm{Tr}(\log([\boldsymbol{M}(\boldsymbol{x})])) \\ &= \mathrm{Tr}\left(\left\{\log([\boldsymbol{N}^{(1)}(\boldsymbol{x})]), \ldots, \log([\boldsymbol{N}^{(p)}(\boldsymbol{x})]), \log(M_{N+1}(\boldsymbol{x})), \ldots, \log(M_n(\boldsymbol{x}))\right\}\right)\end{aligned} \tag{65}$$

for any symmetry class. Next, consider a symmetry class (r is then fixed in the sequel) and let $[\boldsymbol{T}^{(j)}(\boldsymbol{x})] := \log([\boldsymbol{N}^{(j)}(\boldsymbol{x})])$ and $T_k(\boldsymbol{x}) := \log(M_k(\boldsymbol{x}))$. Hence, it is seen that

$$\begin{aligned}\log(\det([\boldsymbol{M}(\boldsymbol{x})])) &= \mathrm{Tr}\left(\left\{[\boldsymbol{T}^{(1)}(\boldsymbol{x})], \ldots, [\boldsymbol{T}^{(p)}(\boldsymbol{x})], T_{N+1}(\boldsymbol{x}), \ldots, T_n(\boldsymbol{x})\right\}\right) \\ &= \sum_{j=1}^{p} \sum_{i=1}^{r(r+1)/2} T_i^{(j)}(\boldsymbol{x}) \, \mathrm{Tr}([E_{\mathcal{I}_r(i,j)}(\boldsymbol{x})]) + \sum_{k=N+1}^{n} T_k(\boldsymbol{x}) \, \mathrm{Tr}([E_k(\boldsymbol{x})])\end{aligned} \tag{66}$$

with

$$[\boldsymbol{T}^{(j)}(\boldsymbol{x})] := \begin{bmatrix} T_1^{(j)}(\boldsymbol{x}) & T_3^{(j)}(\boldsymbol{x}) \\ T_3^{(j)}(\boldsymbol{x}) & T_2^{(j)}(\boldsymbol{x}) \end{bmatrix} \tag{67}$$

if $r = 2$ and

$$[\boldsymbol{T}^{(j)}(\boldsymbol{x})] := \begin{bmatrix} T_1^{(j)}(\boldsymbol{x}) & T_4^{(j)}(\boldsymbol{x}) & T_6^{(j)}(\boldsymbol{x}) \\ T_4^{(j)}(\boldsymbol{x}) & T_2^{(j)}(\boldsymbol{x}) & T_5^{(j)}(\boldsymbol{x}) \\ T_6^{(j)}(\boldsymbol{x}) & T_5^{(j)}(\boldsymbol{x}) & T_3^{(j)}(\boldsymbol{x}) \end{bmatrix} \tag{68}$$

if $r = 3$ (the case $r = 6$ corresponding to the triclinic case is not considered here, since it does not introduce a split between matrix-valued and scalar-valued random fields), and $\mathcal{I}_r(i, j) := (j-1)r(r+1)/2 + i$. Noticing that $\mathrm{Tr}([E_{\mathcal{I}_r(i,j)}(\boldsymbol{x})])$ is indeed independent of the first index i and that $\mathrm{Tr}([E_{\mathcal{I}_r(i,j)}(\boldsymbol{x})]) = 0$ for $\mathcal{I}_r(i, j) > r$, it follows that

$$\log(\det([\boldsymbol{M}(\boldsymbol{x})])) = \sum_{j=1}^{p} \alpha_j \sum_{i=1}^{r} T_i^{(j)}(\boldsymbol{x}) + \sum_{k=N+1}^{n} T_k(\boldsymbol{x}) \, \mathrm{Tr}([E_k(\boldsymbol{x})]) \tag{69}$$

wherein $\alpha_j := \mathrm{Tr}([E_{\mathcal{I}_r(i,j)}(\boldsymbol{x})]) > 0$. Since $\sum_{i=1}^{r} T_i^{(j)}(\boldsymbol{x}) = \mathrm{Tr}([\boldsymbol{T}^{(j)}(\boldsymbol{x})])$ (by construction), it can be deduced that

$$\log(\det(\sum_{i=1}^{n} M_i(\boldsymbol{x})[E^{(i)}(\boldsymbol{x})])) = \sum_{j=1}^{p} \alpha_j \log\left(\det\left([\boldsymbol{N}^{(j)}(\boldsymbol{x})]\right)\right) + \sum_{k=N+1}^{n} \beta_{k-N} \log(M_k(\boldsymbol{x})) \tag{70}$$

with $\beta_{k-N} := \mathrm{Tr}([E_k(\boldsymbol{x})]) > 0$ for $N + 1 \leqslant k \leqslant n$.

Appendix B. Proof of Eq. (40)

Let $[\boldsymbol{D}(\boldsymbol{x})]$ be the random matrix such that

$$[\boldsymbol{D}(\boldsymbol{x})] := [\boldsymbol{M}(\boldsymbol{x})] - [I_6] \tag{71}$$

By using the symbolic forms

$$[\boldsymbol{M}(\boldsymbol{x})] = \left\{[\boldsymbol{N}^{(1)}(\boldsymbol{x})], \ldots, [\boldsymbol{N}^{(p)}(\boldsymbol{x})], M_{N+1}(\boldsymbol{x}), \ldots, M_n(\boldsymbol{x})\right\} \tag{72}$$

and Eq. (11), one has

$$[\boldsymbol{D}(\boldsymbol{x})] = \left\{[\boldsymbol{F}^{(1)}(\boldsymbol{x})], \ldots, [\boldsymbol{F}^{(p)}(\boldsymbol{x})], F_{N+1}(\boldsymbol{x}), \ldots, F_n(\boldsymbol{x})\right\} \tag{73}$$

where the symmetric random matrix $[\boldsymbol{F}^{(j)}(\boldsymbol{x})]$ is given by $[\boldsymbol{F}^{(j)}(\boldsymbol{x})] = [\boldsymbol{N}^{(j)}(\boldsymbol{x})] - [I_r]$ and $F_k(\boldsymbol{x}) = M_k(\boldsymbol{x}) - 1$. It follows that $\|[\boldsymbol{M}(\boldsymbol{x})] - [I_6]\|_F^2 = \mathrm{Tr}([\boldsymbol{D}(\boldsymbol{x})]^{\mathrm{T}}[\boldsymbol{D}(\boldsymbol{x})])$ can be written as

$$\|[\boldsymbol{M}(\boldsymbol{x})] - [I_6]\|_F^2 = \mathrm{Tr}\left\{[\boldsymbol{F}^{(1)}(\boldsymbol{x})]^{\mathrm{T}}[\boldsymbol{F}^{(1)}(\boldsymbol{x})], \ldots, [\boldsymbol{F}^{(p)}(\boldsymbol{x})]^{\mathrm{T}}[\boldsymbol{F}^{(p)}(\boldsymbol{x})], F_{N+1}^2(\boldsymbol{x}), \ldots, F_n^2(\boldsymbol{x})\right\} \tag{74}$$

Let $[\boldsymbol{G}^{(j)}(\boldsymbol{x})]$ be the random matrix such that $[\boldsymbol{G}^{(j)}(\boldsymbol{x})] = [\boldsymbol{F}^{(j)}(\boldsymbol{x})]^{\mathrm{T}}[\boldsymbol{F}^{(j)}(\boldsymbol{x})]$, with

$$[\boldsymbol{G}^{(j)}(\boldsymbol{x})] = \begin{bmatrix} G_1^{(j)}(\boldsymbol{x}) & G_3^{(j)}(\boldsymbol{x}) \\ G_3^{(j)}(\boldsymbol{x}) & G_2^{(j)}(\boldsymbol{x}) \end{bmatrix} \tag{75}$$

for $r = 2$ and

$$[\boldsymbol{G}^{(j)}(\boldsymbol{x})] = \begin{bmatrix} G_1^{(j)}(\boldsymbol{x}) & G_4^{(j)}(\boldsymbol{x}) & G_6^{(j)}(\boldsymbol{x}) \\ G_4^{(j)}(\boldsymbol{x}) & G_2^{(j)}(\boldsymbol{x}) & G_5^{(j)}(\boldsymbol{x}) \\ G_6^{(j)}(\boldsymbol{x}) & G_5^{(j)}(\boldsymbol{x}) & G_3^{(j)}(\boldsymbol{x}) \end{bmatrix} \tag{76}$$

for $r=3$. Proceeding as in Appendix A, it can be deduced that

$$\begin{aligned}\|[\boldsymbol{M}(\boldsymbol{x})]-[I_6]\|_F^2 &= \sum_{j=1}^{p}\sum_{i=1}^{r} G_i^{(j)}(\boldsymbol{x})\,\mathrm{Tr}([E_{\mathcal{I}_r(i,j)}]) + \sum_{k=N+1}^{n} D_k^2(\boldsymbol{x})\,\mathrm{Tr}([E_k(\boldsymbol{x})]) \\ &= \sum_{j=1}^{p}\alpha_j \sum_{i=1}^{r} G_i^{(j)}(\boldsymbol{x}) + \sum_{k=N+1}^{n} D_k^2(\boldsymbol{x})\,\mathrm{Tr}([E_k(\boldsymbol{x})]) \\ &= \sum_{j=1}^{p}\alpha_j \sum_{i=1}^{r}\sum_{\ell=1}^{r} [\boldsymbol{F}^{(j)}]_{i\ell}[\boldsymbol{F}^{(j)}]_{i\ell} + \sum_{k=N+1}^{n} D_k^2(\boldsymbol{x})\,\mathrm{Tr}([E_k(\boldsymbol{x})]) \\ &= \sum_{j=1}^{p}\alpha_j \|[\boldsymbol{F}^{(j)}(\boldsymbol{x})]\|_F^2 + \sum_{k=N+1}^{n} D_k^2(\boldsymbol{x})\,\mathrm{Tr}([E_k(\boldsymbol{x})]) \\ &= \sum_{j=1}^{p}\alpha_j \|[\boldsymbol{N}^{(j)}(\boldsymbol{x})]-[I_r]\|_F^2 + \sum_{k=N+1}^{n} \beta_{k-N}(M_k(\boldsymbol{x})-1)^2\end{aligned} \tag{77}$$

where the sets of integers $\{\alpha_j\}_j$ and $\{\beta_{k-N}\}_k$ are defined in Appendix A. By taking the mathematical expectation on both sides in the equation above, it can be deduced that

$$\mathbb{E}\{\|[\boldsymbol{M}(\boldsymbol{x})]-[I_6]\|_F^2\} = \sum_{j=1}^{p}\alpha_j \|[I_r]\|_F^2\,\delta^2_{[\boldsymbol{N}^{(j)}(\boldsymbol{x})]} + \sum_{k=N+1}^{n}\beta_{k-N}\,\delta^2_{M_k(\boldsymbol{x})} \tag{78}$$

and thus, the dispersion parameter $\delta_{[\boldsymbol{M}]}(\boldsymbol{x})$, defined in Eq. (1), is given by

$$\delta_{[\boldsymbol{M}(\boldsymbol{x})]} = \frac{1}{\sqrt{6}}\left(r\sum_{j=1}^{p}\alpha_j\,\delta^2_{[\boldsymbol{N}^{(j)}(\boldsymbol{x})]} + \sum_{k=N+1}^{n}\beta_{k-N}\,\delta^2_{M_k(\boldsymbol{x})}\right)^{1/2} \tag{79}$$

Appendix C. Tensor bases

In this appendix, the tensor bases and the expression of the dispersion parameter are provided for some symmetry classes (in this work, the modified Voigt notation of these fourth-order tensors has been used). The cases of transversely isotropic and orthotropic materials, which are both considered in the applications, are not recalled hereinafter. As indicated previously, the monoclinic system is not considered here, due to limited applicability.

C.1. Isotropy

The tensor basis is given by

$$[\![E_1]\!] := \frac{1}{3}[I_3]\otimes[I_3], \quad [\![E_2]\!] := [I_3]\boxtimes[I_3] - [\![E_1]\!] \tag{80}$$

and the dispersion parameter reads as

$$\delta_{[\boldsymbol{M}(\boldsymbol{x})]} = \left\{\frac{1}{6}\left(\delta^2_{M_1(\boldsymbol{x})} + 5\delta^2_{M_2(\boldsymbol{x})}\right)\right\}^{1/2} \tag{81}$$

C.2. Cubic

Let $(\boldsymbol{a}(\boldsymbol{x}),\boldsymbol{b}(\boldsymbol{x}),\boldsymbol{c}(\boldsymbol{x}))$ define the crystallographic system at point $\boldsymbol{x}$. The tensor basis is then defined as

$$[\![E_1]\!] := \frac{1}{3}[I_3]\otimes[I_3], \quad [\![E_2(\boldsymbol{x})]\!] := [I_3]\boxtimes[I_3] - [\![S(\boldsymbol{x})]\!], \quad [\![E_3(\boldsymbol{x})]\!] := [\![S(\boldsymbol{x})]\!] - [\![E_1]\!] \tag{82}$$

with

$$[\![S(\boldsymbol{x})]\!] := \boldsymbol{a}(\boldsymbol{x})\otimes\boldsymbol{a}(\boldsymbol{x})\otimes\boldsymbol{a}(\boldsymbol{x})\otimes\boldsymbol{a}(\boldsymbol{x}) + \boldsymbol{b}(\boldsymbol{x})\otimes\boldsymbol{b}(\boldsymbol{x})\otimes\boldsymbol{b}(\boldsymbol{x})\otimes\boldsymbol{b}(\boldsymbol{x}) + \boldsymbol{c}(\boldsymbol{x})\otimes\boldsymbol{c}(\boldsymbol{x})\otimes\boldsymbol{c}(\boldsymbol{x})\otimes\boldsymbol{c}(\boldsymbol{x}) \tag{83}$$

The dispersion parameter is given by:

$$\delta_{[\boldsymbol{M}(\boldsymbol{x})]} = \left\{\frac{1}{6}\left(\delta^2_{M_1(\boldsymbol{x})} + 3\delta^2_{M_2(\boldsymbol{x})} + 2\delta^2_{M_3(\boldsymbol{x})}\right)\right\}^{1/2} \tag{84}$$

C.3. Tetragonal

Let $\boldsymbol{n}(\boldsymbol{x})$ be the unit vector defining the preferred direction of the system, and let $\boldsymbol{a}(\boldsymbol{x})$ and $\boldsymbol{b}(\boldsymbol{x})$ be two unit vectors in $\mathbb{R}^3$ such that $(\boldsymbol{a}(\boldsymbol{x}), \boldsymbol{b}(\boldsymbol{x}), \boldsymbol{n}(\boldsymbol{x}))$ are mutually orthogonal (at point $\boldsymbol{x}$). Moreover, let $[P(\boldsymbol{x})]$ and $[Q(\boldsymbol{x})]$ be the two tensors defined as

$$[P(\boldsymbol{x})] := \boldsymbol{n}(\boldsymbol{x}) \otimes \boldsymbol{n}(\boldsymbol{x}), \quad [Q(\boldsymbol{x})] := [I_3] - [P(\boldsymbol{x})] \tag{85}$$

The basis is given by:

$$\begin{aligned}
&[\![E_1(\boldsymbol{x})]\!] := [P(\boldsymbol{x})] \otimes [P(\boldsymbol{x})], \quad [\![E_2(\boldsymbol{x})]\!] := ([Q(\boldsymbol{x})] \otimes [Q(\boldsymbol{x})])/2 \\
&[\![E_3(\boldsymbol{x})]\!] := ([P(\boldsymbol{x})] \otimes [Q(\boldsymbol{x})] + [Q(\boldsymbol{x})] \otimes [P(\boldsymbol{x})])/\sqrt{2} \\
&[\![E_4(\boldsymbol{x})]\!] := (\boldsymbol{a}(\boldsymbol{x}) \otimes \boldsymbol{b}(\boldsymbol{x}) + \boldsymbol{b}(\boldsymbol{x}) \otimes \boldsymbol{a}(\boldsymbol{x})) \otimes (\boldsymbol{a}(\boldsymbol{x}) \otimes \boldsymbol{b}(\boldsymbol{x}) + \boldsymbol{b}(\boldsymbol{x}) \otimes \boldsymbol{a}(\boldsymbol{x}))/2 \\
&[\![E_5(\boldsymbol{x})]\!] = (\boldsymbol{a}(\boldsymbol{x}) \otimes \boldsymbol{a}(\boldsymbol{x}) - \boldsymbol{b}(\boldsymbol{x}) \otimes \boldsymbol{b}(\boldsymbol{x})) \otimes (\boldsymbol{a}(\boldsymbol{x}) \otimes \boldsymbol{a}(\boldsymbol{x}) - \boldsymbol{b}(\boldsymbol{x}) \otimes \boldsymbol{b}(\boldsymbol{x}))/2 \\
&[\![E_6(\boldsymbol{x})]\!] := [P(\boldsymbol{x})] \boxtimes [Q(\boldsymbol{x})] + [Q(\boldsymbol{x})] \boxtimes [P(\boldsymbol{x})]
\end{aligned} \tag{86}$$

Furthermore, the dispersion parameter writes

$$\delta_{[\boldsymbol{M}(\boldsymbol{x})]} = \left\{ \frac{1}{6} \left(2\delta^2_{[\boldsymbol{N}^{(1)}(\boldsymbol{x})]} + \delta^2_{M_4(\boldsymbol{x})} + \delta^2_{M_5(\boldsymbol{x})} + 2\delta^2_{M_6(\boldsymbol{x})} \right) \right\}^{1/2} \tag{87}$$

C.4. Trigonal

Let $\boldsymbol{n}(\boldsymbol{x})$ be the unit vector orthogonal to the plan spanned by the unit vectors $\boldsymbol{a}(\boldsymbol{x})$ and $\boldsymbol{b}(\boldsymbol{x})$, and assume that an angle of $2\pi/3$ is left between these two vectors in that plane (at point $\boldsymbol{x}$). Let us introduce the following tensors:

$$\begin{aligned}
&[P(\boldsymbol{x})] := \boldsymbol{n}(\boldsymbol{x}) \otimes \boldsymbol{n}(\boldsymbol{x}), \quad [Q(\boldsymbol{x})] := [I_3] - [P(\boldsymbol{x})] \\
&[S(\boldsymbol{x})] := \sqrt{2/3}\,(\boldsymbol{a}(\boldsymbol{x}) \otimes \boldsymbol{a}(\boldsymbol{x}) + \boldsymbol{a}(\boldsymbol{x}) \otimes \boldsymbol{b}(\boldsymbol{x}) + \boldsymbol{b}(\boldsymbol{x}) \otimes \boldsymbol{a}(\boldsymbol{x})) \\
&[T(\boldsymbol{x})] := \sqrt{2/3}\,(\boldsymbol{b}(\boldsymbol{x}) \otimes \boldsymbol{b}(\boldsymbol{x}) + \boldsymbol{a}(\boldsymbol{x}) \otimes \boldsymbol{b}(\boldsymbol{x}) + \boldsymbol{b}(\boldsymbol{x}) \otimes \boldsymbol{a}(\boldsymbol{x})) \\
&[U(\boldsymbol{x})] := (\boldsymbol{n}(\boldsymbol{x}) \otimes \boldsymbol{a}(\boldsymbol{x}) + \boldsymbol{a}(\boldsymbol{x}) \otimes \boldsymbol{n}(\boldsymbol{x}))/\sqrt{2}, \quad [V(\boldsymbol{x})] := -(\boldsymbol{n}(\boldsymbol{x}) \otimes \boldsymbol{b}(\boldsymbol{x}) + \boldsymbol{b}(\boldsymbol{x}) \otimes \boldsymbol{n}(\boldsymbol{x}))/\sqrt{2} \\
&[W(\boldsymbol{x})] := (4/3)([S(\boldsymbol{x})] \otimes [U(\boldsymbol{x})] + [T(\boldsymbol{x})] \otimes [V(\boldsymbol{x})] - (1/2)[T(\boldsymbol{x})] \otimes [U(\boldsymbol{x})] - (1/2)[S(\boldsymbol{x})] \otimes [V(\boldsymbol{x})]) \\
&[Z(\boldsymbol{x})] := (4/3)([U(\boldsymbol{x})] \otimes [S(\boldsymbol{x})] + [V(\boldsymbol{x})] \otimes [T(\boldsymbol{x})] - (1/2)[U(\boldsymbol{x})] \otimes [T(\boldsymbol{x})] - (1/2)[V(\boldsymbol{x})] \otimes [S(\boldsymbol{x})])
\end{aligned} \tag{88}$$

The basis is then defined by the following tensors:

$$\begin{aligned}
&[\![E_1(\boldsymbol{x})]\!] := [P(\boldsymbol{x})] \otimes [P(\boldsymbol{x})] \\
&[\![E_2(\boldsymbol{x})]\!] := ([Q(\boldsymbol{x})] \otimes [Q(\boldsymbol{x})])/2 \\
&[\![E_3(\boldsymbol{x})]\!] := ([P(\boldsymbol{x})] \otimes [Q(\boldsymbol{x})] + [Q(\boldsymbol{x})] \otimes [P(\boldsymbol{x})])/\sqrt{2} \\
&[\![E_4(\boldsymbol{x})]\!] := (4/3)([S(\boldsymbol{x})] \otimes [S(\boldsymbol{x})] + [T(\boldsymbol{x})] \otimes [T(\boldsymbol{x})] - (1/2)[S(\boldsymbol{x})] \otimes [T(\boldsymbol{x})] - (1/2)[T(\boldsymbol{x})] \otimes [S(\boldsymbol{x})]) \\
&[\![E_5(\boldsymbol{x})]\!] := (4/3)([U(\boldsymbol{x})] \otimes [U(\boldsymbol{x})] + [V(\boldsymbol{x})] \otimes [V(\boldsymbol{x})] - (1/2)[U(\boldsymbol{x})] \otimes [V(\boldsymbol{x})] - (1/2)[V(\boldsymbol{x})] \otimes [U(\boldsymbol{x})]) \\
&[\![E_6(\boldsymbol{x})]\!] := [W(\boldsymbol{x})] + [Z(\boldsymbol{x})]
\end{aligned} \tag{89}$$

The dispersion parameter reads as

$$\delta_{[\boldsymbol{M}(\boldsymbol{x})]} = \left\{ \frac{1}{3} \left(\delta^2_{[\boldsymbol{N}^{(1)}(\boldsymbol{x})]} + 2\delta^2_{[\boldsymbol{N}^{(2)}(\boldsymbol{x})]} \right) \right\}^{1/2} \tag{90}$$

Appendix D. Derivation of the covariance kernel for constant scaling and diffusion fields

Let us consider the following SDE in $\mathbb{R}^3$ (see [25] for the solution in $\mathbb{R}^2$):

$$\left[\kappa^2 - \langle \nabla, [D]\nabla \rangle \right] \Xi_k(\boldsymbol{x}) = \mathcal{W}(\boldsymbol{x}), \quad \forall \boldsymbol{x} \in \mathbb{R}^3 \tag{91}$$

where the power spectral density of $\mathcal{W}$ is $1/(2\pi)^3$. Since the scaling parameter κ and the diffusion field $[D]$ are both constant over $\mathbb{R}^3$, the solution is stationary and its power spectral density writes

$$S_k(\boldsymbol{\omega}) = \frac{1}{(2\pi)^3} \times \frac{1}{(\kappa^2 + \langle \boldsymbol{\omega}, [D]\boldsymbol{\omega} \rangle)^2} \tag{92}$$

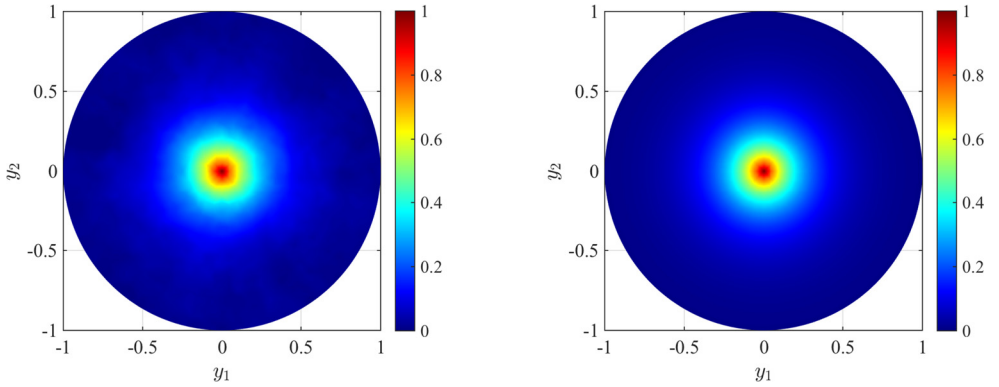

Fig. 11. The graph of the correlation function $(y_1, y_2) \mapsto R_1((0,0,1.5),(y_1,y_2,1.5))$ is shown in the left panel for $\kappa(\boldsymbol{x}) = 5$ and $[D(\boldsymbol{x})] = [I_3]$. The right panel displays the theoretical result given by Eq. (50).

Owing to the slight abuse of notation $R_k(\boldsymbol{x},\boldsymbol{y}) = R_k(\boldsymbol{h})$, with $\boldsymbol{h} := \boldsymbol{x} - \boldsymbol{y}$, the associated covariance function R_k is then given by

$$R_k(\boldsymbol{h}) = \frac{1}{(2\pi)^3} \int_{\mathbb{R}^3} \frac{\exp(\mathrm{i}\langle \boldsymbol{\omega}, \boldsymbol{h}\rangle)}{(\kappa^2 + \langle \boldsymbol{\omega}, [D]\boldsymbol{\omega}\rangle)^2}\, \mathrm{d}\boldsymbol{\omega} \tag{93}$$

Upon using the transformation $\boldsymbol{s} = \kappa^{-1}\,[D]^{1/2}\,\boldsymbol{\omega}$ (where $[D] > 0$ by definition) [25], one has

$$R_k(\boldsymbol{h}) = \frac{1}{(2\pi)^3} \int_{\mathbb{R}^3} \frac{\exp(\kappa\,\mathrm{i}\,\langle \boldsymbol{h}, [D]^{-1/2}\boldsymbol{s}\rangle)}{\kappa^4(1+\|\boldsymbol{s}\|^2)^2}\, \det(\kappa[D]^{-1/2})\, \mathrm{d}\boldsymbol{s} \tag{94}$$

and thus

$$R_k(\boldsymbol{h}) = \frac{1}{(2\pi)^3 \kappa \sqrt{\det([D])}} \int_{\mathbb{R}^3} \frac{\exp(\kappa\,\mathrm{i}\,\langle [D]^{-\mathrm{T}/2}\,\boldsymbol{h}, \boldsymbol{s}\rangle)}{(1+\|\boldsymbol{s}\|^2)^2}\, \mathrm{d}\boldsymbol{s} \tag{95}$$

Let $\boldsymbol{z} := \kappa\,[D]^{-\mathrm{T}/2}\,\boldsymbol{h}$, so that $R_k(\boldsymbol{h}) = \widehat{R}_k(\boldsymbol{z})$ with

$$\widehat{R}_k(\boldsymbol{z}) = \frac{1}{(2\pi)^3 \kappa \sqrt{\det([D])}} \int_{\mathbb{R}^3} \frac{\exp(\mathrm{i}\langle \boldsymbol{s}, \boldsymbol{z}\rangle)}{(1+\|\boldsymbol{s}\|^2)^2}\, \mathrm{d}\boldsymbol{s} \tag{96}$$

By using the spherical coordinate system (r,θ,ϕ), where ϕ denotes the angle between $\boldsymbol{z}/\|\boldsymbol{z}\|$ and $\boldsymbol{s}$, it can be shown that

$$\widehat{R}_k(\boldsymbol{z}) = \frac{1}{(2\pi)^3 \kappa \sqrt{\det([D])}} \int_{r=0}^{+\infty} \int_{\theta=0}^{2\pi} \int_{\phi=0}^{\pi} \frac{r^2}{(1+r^2)^2} \sin(\phi) \exp\left(\mathrm{i}\, r\, \|\boldsymbol{z}\| \cos(\phi)\right)\, \mathrm{d}r\, \mathrm{d}\theta\, \mathrm{d}\phi \tag{97}$$

It can then be deduced that the covariance function writes

$$R_k(\boldsymbol{h}) = \frac{1}{8\pi\kappa \sqrt{\det([D])}} \exp\left(-\kappa\, \|[D]^{-1/2}\,\boldsymbol{h}\|\right) \tag{98}$$

This result is illustrated in Fig. 11 for the geometry introduced in Sec. 3.2. Here, the covariance kernel $(\boldsymbol{x},\boldsymbol{y}) \mapsto R_1(\boldsymbol{x},\boldsymbol{y})$ estimated (from 20,000 simulations on the *bounded* domain Ω) for $\boldsymbol{x} = (0,0,1.5)$ and $\boldsymbol{y} = (y_1, y_2, 1.5)$ is compared with the theoretical result given by Eq. (50).

References

[1] A. Nouy, C. Soize, Random field representations for stochastic elliptic boundary value problems and statistical inverse problems, Eur. J. Appl. Math. 25 (03) (2014) 339–373.
[2] C. Soize, Non-Gaussian positive-definite matrix-valued random fields for elliptic stochastic partial derivative operators, Comput. Methods Appl. Mech. Eng. 195 (2006) 26–64.
[3] M. Grigoriu, Probabilistic models for stochastic elliptic partial differential equations, J. Comput. Phys. 229 (2010) 8406–8429.
[4] P. Ciarlet, Mathematical Elasticity, vol. I: Three-Dimensional Elasticity, Elsevier Science Publishers, 1988.
[5] M. Grigoriu, Microstructure models and material response by extreme value theory, SIAM/ASA J. Uncertain. Quantificat. 4 (1) (2016) 190–217.
[6] E. Jaynes, Information theory and statistical mechanics I, Phys. Rev. 106 (4) (1957) 620–630.

[7] E. Jaynes, Information theory and statistical mechanics II, Phys. Rev. 108 (2) (1957) 171–190.
[8] J. Guilleminot, A. Noshadravan, C. Soize, R. Ghanem, A probabilistic model for bounded elasticity tensor random fields with application to polycrystalline microstructures, Comput. Methods Appl. Mech. Eng. 200 (2011) 1637–1648.
[9] J. Guilleminot, C. Soize, On the statistical dependence for the components of random elasticity tensors exhibiting material symmetry properties, J. Elast. 111 (2013) 109–130.
[10] J. Guilleminot, C. Soize, Stochastic model and generator for random fields with symmetry properties: application to the mesoscopic modeling of elastic random media, SIAM J. Multiscale Model. Simul. 11 (2013) 840–870.
[11] B. Staber, J. Guilleminot, Approximate solutions of Lagrange multipliers for information-theoretic random field models, SIAM/ASA J. Uncertain. Quantificat. 3 (2015) 599–621.
[12] A. Malyarenko, M. Ostoja-Starzewski, A random field formulation of Hooke's law in all elasticity classes, J. Elast. 34 (2) (2017) 269–302.
[13] M. Ostoja-Starzewski, Microstructural Randomness and Scaling in Mechanics of Materials, Modern, Mechanics and Mathematics Series, Chapman & Hall/CRC/Taylor & Francis, 2008.
[14] C. Soize, A nonparametric model of random uncertainties for reduced matrix models in structural dynamics, Probab. Eng. Mech. 15 (3) (2000) 277–294.
[15] J. Guilleminot, C. Soize, Stochastic modeling of anisotropy in multiscale analysis of heterogeneous materials: a comprehensive overview on random matrix approaches, Mech. Mater. 44 (2012) 35–46.
[16] M.M. Mehrabadi, S.C. Cowin, Eigentensors of linear anisotropic elastic materials, Q. J. Mech. Appl. Math. 43 (1) (1990) 15–41.
[17] I. Babuška, R. Tempone, G.E. Zouraris, Solving elliptic boundary value problems with uncertain coefficients by the finite element method: the stochastic formulation, Comput. Methods Appl. Mech. Eng. 194 (2005) 1251–1294.
[18] J. Guilleminot, C. Soize, Generalized stochastic approach for constitutive equation in linear elasticity: a random matrix model, Int. J. Numer. Methods Biomed. Eng. 90 (5) (2012) 613–635.
[19] L. Walpole, Fourth-rank tensors on the thirty-two crystal classes: Multiplication tables, Proc. R. Soc. Lond. A 391 (1984) 149–179.
[20] R. Balian, Random matrices and information theory, Il Nuovo Cimento B 57 (1) (1968) 183–193.
[21] S. Boyd, L. Vandenberghe, Convex Optimization, Cambridge University Press, 2004.
[22] R.M. Dudley, The size of compact subsets of Hilbert spaces and continuity of Gaussian processes, J. Funct. Anal. 1 (1967) 290–330.
[23] J. Guilleminot, C. Soize, Itô SDE–based generator for a class of non-Gaussian vector-valued random fields in uncertainty quantification, SIAM J. Sci. Comput. 36 (2014) A2763–A2786.
[24] F. Lindgren, H. Rue, J. Lindström, An explicit link between Gaussian fields and Gaussian Markov random fields: the stochastic partial differential equation approach, J. R. Stat. Soc., Ser. B, Stat. Methodol. 74 (4) (2011) 423–498.
[25] G.-A. Fuglstad, D. Simpson, F. Lindgren, H. Rue, Exploring a new class of nonstationary spatial Gaussian random fields with varying local anisotropy, Stat. Sin. 133 (2015) 25–115.
[26] G.-A. Fuglstad, D. Simpson, F. Lindgren, H. Rue, Does non-stationary spatial data always require non-stationary random fields?, Spat. Stat. 14 (2015) 505–531.
[27] T.-T. Le, J. Guilleminot, C. Soize, Stochastic continuum modeling of random interphases from atomistic simulations. Application to a polymer nanocomposite, Comput. Methods Appl. Mech. Eng. 303 (2016) 430–449.